Scattering and absorption properties of near-surface aerosol over Gangetic-Himalayan region: the role of boundary layer dynamics and long-range transport

U. C. Dumka[1*] D. G. Kaskaoutis[2], M. K. Srivastava[3] and P. C. S. Devara[4]

[1]Aryabhatta Research Institute of Observational Sciences, Nainital, India

[2]Department of Physics, School of Natural Sciences, Shiv Nadar University, Tehsil Dadri, India

[3]Department of Geophysics, Banaras Hindu University, Varanasi, India

[4]Amity Institute of Laser Technology & Optoelectronics, Amity University Haryana, Gurgaon (Manesar), India

*Correspondence to: U. C. Dumka (dumka@aries.res.in; ucdumka@gmail.com)

Abstract

Light scattering and absorption properties of atmospheric aerosols are of vital importance in evaluating their types, sources and radiative forcing. This is of particular interest over the Gangetic-Himalayan (GH) region due to uplift of aerosol from the plains to the Himalayan range causing serious effects on atmospheric heating, glaciology and monsoon circulation. In this respect, Ganges Valley Aerosol Experiment (GVAX) was initiated at Nainital during June 2011 to March 2012 aiming to examine the aerosol properties, source regions, uplift mechanisms and aerosol-radiation-cloud interactions. The present study examines the temporal (diurnal, monthly, seasonal) evolution of scattering (σ_{sp}) and absorption (σ_{ap}) coefficients, their wavelength dependence, and the role of the Indo-Gangetic plains (IGP), boundary-layer dynamics (BLD) and long-range transport (LRT) in aerosol evolution via the Atmospheric Radiation Measurement Mobile Facility. The analysis is separated for particles <10 μm and <1 μm in diameter in order to examine the influence of the particle size on optical properties. The σ_{sp} and σ_{ap} exhibit a pronounced seasonal variation with monsoon low and post-monsoon (November) high, while the scattering wavelength exponent exhibits higher values during monsoon, in contrast to the absorption Ångström exponent which maximizes in December-March. The elevated-background measuring site provides the advantage of examining the LRT of natural and anthropogenic aerosols from the IGP and southwest Asia and the role of BLD in the aerosol lifting processes. The results reveal higher aerosol concentrations during noontime along with increase in mixing height suggesting influence from IGP. The locally-emitted aerosols present higher wavelength dependence of the absorption during October to March period compared to the rather well-mixed and aged transported aerosols. Monsoon rainfall and seasonally-changing air masses contribute to the alteration of the extensive and intensive aerosol properties.

1. Introduction

Light scattering and absorption by atmospheric aerosol cause reduction in solar radiation reaching the ground and deterioration of visibility and air quality, modifying the atmosphere's radiative and energy budget (Antón et al., 2012). On the other hand, the backscattering ratio is a crucial variable for quantifying the cooling effect of aerosols on climate. Although it is weakly dependent on aerosol concentration, it provides useful information of the refractive index, angular dependence of scattering, size and shape of aerosols (Gopal et al., 2014). Wide-spread aerosol pollution mostly from anthropogenic sources is a common phenomenon over the south Asia, with serious effects on atmospheric circulation, climate and human health (Lawrence and Lelieveld, 2010 and references therein). This aerosol-pollution layer, especially over the Indo-Gangetic Plains (IGP), is clearly observed by the satellite imagery as a thick haze layer (Atmospheric Brown Clouds, ABC) over the region (Di Girolamo et al., 2004; Ramanathan et al., 2007), spreading also over the Himalayas with significant light absorption due to large Black Carbon (BC) concentration (Adhikary et al., 2007; Nakajima et al., 2007; Kopacz et al., 2010; Gautam et al., 2011).

During the last decades, the IGP has experienced increasing aerosol and pollutant emissions mainly from anthropogenic sources, fossil-fuel and bio-fuel combustion and agricultural biomass burning (Lu et al., 2011; Kaskaoutis et al., 2012), which along with the natural dust emissions and long-range transport (LRT) have led to severe turbid atmospheres (Kaskaoutis et al., 2013). As a consequence, aerosols can strongly modify the regional climate via radiative forcing (Ramanathan et al., 2005; Lau et al., 2006; Gautam et al., 2010) and changes in cloud microphysics, monsoon rainfall and dynamics (Randles and Ramaswamy, 2008, Bollasina and Nigam, 2009; Ganguly et al., 2012; Manoj et al., 2011; Dipu et al., 2013). Due to their significant influence on regional weather, climate, monsoon circulation, glaciology and human health, aerosols are systematically examined over Indian Himalayas, mostly focusing on columnar properties and radiative forcing (Dumka et al., 2006, 2008; Hegde et al., 2007; Guleria et al., 2011 and reference therein) and a few studies on aerosol chemistry (Ram et al., 2008, 2010; Hegde and Kawamura, 2012). On the other hand, systematic analysis of near-surface aerosol properties is sparse and mostly performed under an Indian-Finish research initiative (Hyvärinen et al., 2009, 2011a, 2011b). Furthermore, Raatikainen et al. (2014) examined the influence of boundary-layer dynamics (BLD) and the effect of changes in boundary-layer height (BLH) on aerosol concentrations over the IGP and their transport up to the Himalayas foothills. Panwar et al. (2013) analyzed the evolution of the PM and BC aerosol mass concentrations at Mukteshwar with respect to seasonal variations of BLH, while Komppula et al. (2009) and

Neitola et al. (2011) focused on the aerosol size distribution and new particle formation at the same site. These studies corroborate larger aerosol concentrations and new particle formation during the spring period associated with higher BLH and increased influence of transported aerosols.

To improve the knowledge of radiative properties of atmospheric aerosols, their origin and spatio-temporal distribution over the Gangetic-Himalayan (GH) region, the Ganges Valley Aerosol Experiment (GVAX) was initiated during June 2011 to March 2012 (Kotamarthi and Satheesh, 2011). The GVAX project was a joint research campaign between US Department of Energy (DoE) Atmospheric Radiation Measurement (ARM) Program and Indian Institute of Science, Bangalore conducted at Manora Peak, Nainital, in the central part of Indian Himalayas (29.21^{o} N, 79.27^{o} E, 1958 m a.m.s.l). Based on GVAX measurements, Manoharan et al. (2014) analyzed the aerosol properties, mostly emphasizing on the higher absorption of the super-micron (1-10 µm) particles during October-November accounting for 44% of the total aerosol radiative forcing. Dumka and Kaskaoutis (2014) examined the variation of the single scattering albedo (SSA) during GVAX and its contribution to the aerosol radiative forcing efficiency depending on particle size, also discussing some preliminary results of the monthly variation of scattering and absorption coefficients.

The present work aims to a comprehensive investigation of the intensive and extensive aerosol properties (scattering, backscattering and absorption coefficients, their wavelength dependence and relationships between them) as a function of particle size ($D_{10\mu m}$ and $D_{1\mu m}$) over the GH region during the GVAX campaign. The main objective is to shed light in the temporal (daily, monthly, seasonal) evolution of the near-surface aerosol properties and the specific role of the BLD, uplift of aerosols, LRT and rainy washout. The nearly background measuring site (Nainital), gives us the possibility of exploring the specific role of aerosol-pollution uplift from the IGP to the Himalayan foothills and the seasonal influence of the LRT on aerosol optical properties.

2. Measurements and data analysis

2.1. Observational site

The aerosol measurements were conducted by DoE/ARM Mobile Facility (AMF) deployed at the mountain-top (1958 m amsl) Manora Peak, Nainital, in the GH region (Dumka and Kaskaoutis, 2014). The observational site is far from any major pollution sources, such as industrialized areas and metropolitan cities, with a total population of ~0.5 million and density of ~50 people per km^2

(census 2011). The site is bounded by high-altitude mountain peaks in the north and east directions and opens to the IGP region (densely populated, high polluted and aerosol laden) in the south and west. By considering the elevated nature of the site, the growth of planetary boundary layer (PBL) in the early afternoon hours (usually up to 3-3.5 km amsl) plays a major role in bringing-up aerosols from the IGP, causing significant perturbations in atmospheric physics and chemistry (Dumka et al., 2010; Prabha et al., 2012). The major aerosol sources at Nainital during winter are local/regional biomass-burning emissions (domestic use and heating purposes) and transport of pollutants from the IGP (Dumka et al., 2008). During pre-monsoon (March–June), the site is influenced by transported dust plumes from Thar desert and southwest Asia (Hegde et al., 2007; Kumar et al., 2014) with a relative decrease in carbonaceous aerosols (Ram et al., 2008), while in post-monsoon, smoke-laden air masses from agricultural crop-residue burning in Punjab affect the site. Rain-washout process during the monsoon period decreases the aerosol concentration.

2.2. Measurements and techniques

In-situ measurements of near-surface aerosol absorption (σ_{ap}) and scattering (σ_{sp}) coefficients were carried out using the aerosol observing system (AOS) (Sheridan et al., 2001; Jefferson, 2011 and reference therein). The AOS was housed in an air conditioned trailer and aerosol samples were obtained from the top of a stainless steel intake stack (20.3 cm inner diameter), protected with a rain cap. The aerosols were passed from the stack through a manifold and into several sampling lines that deliver the sample air to the various instruments. Each aerosol sample passes through switched impactors that toggle the aerosol size cut between 1.0 µm ($D_{1\mu m}$) and 10 µm ($D_{10\mu m}$) aerodynamic particle diameters every 30 minutes, thus allowing the examination of both fine and coarse particles (Jefferson, 2011). The AOS instrumentation that is used in the current work consists of Nephelometer and Particle Soot Absorption Photometer (PSAP) from which several extensive and intensive aerosol properties have been analyzed (see Table 1).

The σ_{ap} was measured via the three wavelengths (0.47, 0.53 and 0.66 µm) PSAP. The PSAP uses a filter-based technique in which aerosols are continuously deposited onto a glass fibre filter and the change in the transmitted light is related to the σ_{ap} of the deposited particles using the Lambert Beer's law (Bond et al., 1999). The filter was changed whenever the amount of transmitting light achieved is ~70% of the initial intensity, while the data averaging time was 1 minute. The response of PSAP depends on aerosol loading on the filter, amount of light scattered by particles, flow rate (~0.8 lpm) and spot size (Virkkula et al., 2011). Following the methodology from several previous works (Bond et al., 1999; Ogren, 2010; Virkkula et al.,

2011), the raw PSAP data were processed to estimate the σ_{ap} by incorporating the sample area, flow rate and spot size calibrations. Other biases are due to the scattering and multi-sample loading on the filter, instrument noise (~6% of total absorption, Bond et al., 2001) and uncertainty in the PSAP measurements (1 to 4 Mm^{-1} for the 1-min averaged data samples, Manoharan et al., 2014). The total uncertainty of the PSAP measurements after the transmission and scattering correction is ~20-30% (Bond et al., 1999).

The total scattering (σ_{sp}; between 7^o and 170^o) and hemispheric backscattering (σ_{bsp}; between 90^o and 170^o) coefficients at three wavelengths (0.45, 0.55 and 0.70 µm) were measured with an integrating Nephelometer (Model 3563, TSI). The Nephelometer operated at a relative humidity (RH) below 40% to minimize the effects of changing RH on measurements, while a second Nephelometer was also connected to a humidity scanning system to provide measurements of σ_{sp} and σ_{bsp} as a function of RH for studying the light scattering enhancement factor (work under preparation). The angular non-idealities (i.e. truncation error) and non-Lambertian light source were corrected following the methodology described by Anderson and Ogren (1998) and details given in Dumka and Kaskaoutis (2014 and references therein). These corrections are needed to subtract the light scattering by air molecules, the instrument walls and the detector background noise. The averaging time was set to 1 min, and the Nephelometer was calibrated using CO_2 as high span gas and air as low span gas. On an average, the calibration constant is within ± 2 % and the overall uncertainty in the σ_{sp} is ~7% (Heintzenberg et al., 2006). However, as noticed at the end of the campaign, the CO_2 was of low quality to produce an accurate calibration, thus increasing the uncertainty of the Nephelometer measurements to 10-15%.

The aerosol coefficients σ_{ap}, σ_{bsp} and σ_{sp} measured directly by the AOS are referred as "extensive properties", because they are mainly pertain to the amount of aerosols in the atmosphere. These measurements were used to determine several other aerosol variables (known as "intensive properties"), such as hemispheric backscatter fraction (b), scattering Ångström exponent (SAE), absorption Ångström exponent (AAE), sub-micron scattering (R_{sp}) and absorption (R_{ap}) fractions, which are involved in the radiative forcing estimations, rather than being related directly to the aerosol loading (Table 1). Therefore, the intensive properties relate more to the character of aerosols, such as albedo, particle size and hygroscopic behavior.

3. Results and discussion

3.1. Variations in meteorological variables

In terms of weather conditions and climatology, the observational site is characterized by four different seasons: winter (December-January-February; DJF), spring/pre-monsoon (March-April-May; MAM), summer/monsoon (June-July-August-September; JJAS) and autumn/post-monsoon (October-November; ON), respectively. The ambient pressure, temperature (Temp), relative humidity (RH), wind speed (WS) and wind direction (WD) were continuously monitored during the study period (June 2011 to March 2012) using the surface meteorological instrumentation (MET) data from the ARM AMF facility.

The ambient atmospheric pressure varies between 79 and 81 Kpa, gradually increasing from monsoon to winter and then, slightly decreasing towards spring (Fig. 1a). The monthly-mean temperature remains nearly steady (~20 ^{o}C) between June and September, with a gradual decrease thereafter to a minimum value of ~ 7 ^{o}C in January (Fig. 1b). The RH is greater than 90% during summer monsoon and decreases to about 60% to 40% during the rest of the period, also exhibiting larger fluctuation due to changing weather conditions involving arrival of humid or dry air masses (Fig. 1c). In general, the wind speed (Fig. 1d) varies between 2 and 6 m s^{-1} with an average of ~ 2 m s^{-1} for most of the time. Westerly-to-northwesterly winds (Fig. 1e) dominate during October-March period, carrying aerosols and pollutants from western IGP and southwest Asia. June is mostly considered as a transition month with changing wind from westerly to easterly, while the mean wind direction from July to September is easterly to south-easterly associated with increased monsoon rainfall.

3.2. Temporal evolution of near-surface aerosol properties

This section analyzes the temporal evolution of near-surface aerosol properties at Nainital and discusses them as a function of wavelength, particle size and prevailing atmospheric and meteorological conditions.

3.2.1. Extensive properties

The mean values (averaged during the entire study period) of spectral σ_{sp}, σ_{bsp} and σ_{ap} for $D_{1\mu m}$ and $D_{10\mu m}$ are shown in Fig. 2 (a-c). It should be noted that the properties of $D_{1\mu m}$ particles are also included in the $D_{10\mu m}$, but with much lesser contribution; thus, separate analysis of $D_{1\mu m}$ and $D_{10\mu m}$ will reveal the influence of particle size on aerosol extensive and intensive properties. All the examined variables present a slight decreasing trend with wavelength, but the largest differences are seen as a function of the particle size, since $D_{10\mu m}$ particles exhibit higher scattering, backscattering and absorption as well. On the other hand, the range of all variables is larger for $D_{10\mu m}$ particles since their size distribution is much more expanded, suggesting larger

variability in source regions, mixing processes and optical properties. Although such a behavior is expected for the scattering and backscattering processes via the Mie theory (the larger particles are more efficient scatters especially at longer wavelengths), the higher absorption by the larger particles is an important finding of the GVAX campaign. Manoharan et al. (2014) reported a 30% greater absorption for $D_{10\mu m}$ compared to $D_{1\mu m}$ during October–November 2011, in contrast to the similar values (7.63 ± 5.32 and 6.38 ± 3.91 for $D_{10\mu m}$ and $D_{1\mu m}$, respectively) during monsoon. The post-monsoon season coincides with the post-harvest agricultural biomass burning period in Punjab, northwestern India (Kaskaoutis et al., 2014), implying that the absorbing aerosols can be also of larger size due to atmospheric mixing and ageing processes (gas-to-particle conversion, coagulation, condensation) during their transportation up to Nainital. These aerosols are mostly emitted over IGP, whereas the local freshly-emitted aerosols at Nainital (mostly in the $D_{1\mu m}$ size) seem not to affect so much the light absorption due to their significantly lower abundance (Hyvärinen et al., 2009; Ram et al., 2010). It should be noted that the difference in absorption coefficient between $D_{10\mu m}$ and $D_{1\mu m}$ was found to be larger for higher aerosol loading. On the other hand, the scattering is much larger (~ 40%) for the $D_{10\mu m}$, especially at longer wavelengths, while the σ_{bsp} exhibits rather neutral wavelength dependence. The monthly variation of the spectral σ_{sp} and σ_{ap} was documented in Dumka and Kaskaoutis (2014).

The average σ_{sp} and σ_{ap} during the whole study period were found to be 177.2 Mm^{-1} and 10.9 Mm^{-1}, respectively, for the $D_{10\mu m}$ and 104.4 Mm^{-1} and 8.95 Mm^{-1} for the $D_{1\mu m}$ (Table 2), with significant seasonal variation, which is examined in the following. The mean value of σ_{sp} is similar to earlier observations over the site (Pant et al., 2006; Beegum et al., 2009). The σ_{sp} values over central Indian Himalayas (present study and Hyvärinen et al. 2009) are comparable to those found over central India during February 2004 (Jayaraman et al., 2006), but much lower than those (250 - 2000 Mm^{-1}) reported at polluted Indian megacities, like Delhi (Ganguly et al., 2006). Lower values of σ_{sp} (97±9 Mm^{-1}) and higher of σ_{bsp} (14 ± 1 Mm^{-1}) at 550 nm compared to Nainital were found in Anantapur, south India during January – December 2011 (Gopal et al., 2014), suggesting dominance of different aerosol types. σ_{sp} value of 75 ± 42 Mm^{-1} at 550 nm was reported by Andreae et al. (2002) at Sde Boker, Israel, which was typical of moderate-polluted continental air masses, while values of 26 Mm^{-1} and 410 Mm^{-1} were found for clean and heavy-smog days, respectively, in Los Angeles (Seinfeld and Pandis, 1998). Table 2 summarizes the extensive and intensive aerosol properties over Nainital during the GVAX campaign along with those measured over mountainous and remote sites over the globe. The comparison shows that Nainital, although its elevated terrain and remoteness from urban and industrialized regions,

usually receives substantial amounts of anthropogenic aerosols, in addition to mineral dust and biomass burning, rendering the site as moderately polluted.

3.2.2. Intensive properties

The monthly values of SAE and AAE determined at three spectral bands are shown in Figs. 3 and 4, respectively, for both $D_{1\mu m}$ and $D_{10\mu m}$ size groups. Starting from the SAE (Fig. 3), a similar temporal variation is revealed for both size groups, but with much larger values for the $D_{1\mu m}$ (mean of 1.21 ± 0.35 at 0.45-0.70 µm) compared to $D_{10\mu m}$ (mean of 0.72 ± 0.42 at 0.45-0.70 µm). The SAE follows an anti-correlation with the coarse-to-fine mode ratio exhibiting much higher values for sub-micron aerosols, especially at shorter wavelengths (Andreae et al., 2002). The wide range (~0.1 to 2.4) of SAE values for both particle groups suggests large variability in sources, seasonality and mixing processes at the measuring site. The spectral $D_{1\mu m}/D_{10\mu m}$ SAE ratio is nearly constant to 1.68 suggesting that $D_{10\mu m}$ particles possess higher scattering at longer wavelengths leading to a more neutral spectrum (Manoharan et al., 2014). The average value of SAE at 0.45-0.70 µm was found to be 1.02 ± 0.30 at Anantapur (Gopal et al., 2014), which is well within the average values of $D_{1\mu m}$ and $D_{10\mu m}$ at Nainital. Furthermore, the SAE values are higher at the shorter wavelength bands, suggesting higher decreasing rate of the scattering process at shorter wavelengths, as expected from the Mie theory. Thus, despite the fact that $D_{1\mu m}$ and $D_{10\mu m}$ particles exhibit similar annual pattern for scattering and absorption (Dumka and Kaskaoutis 2014), the values and the wavelength dependence may be quite different, indicating that the particle size plays a prominent role in altering the aerosol optical properties and wavelength dependence.

The monthly variability depends on the dominant aerosol type, the contribution of local and transported aerosols, the prevailing meteorological conditions and the mixing processes in the atmosphere. The maximum monthly-mean SAE is observed in August (1.11 ± 0.31 and 1.53 ± 0.26 for $D_{10\mu m}$ and $D_{1\mu m}$, respectively) and, in general, the wavelength dependence of scattering seems to be higher during monsoon. On the other hand, the minimum values are shown in October and November, when the site is under significant influence of the smoke-laden air masses from northwestern India, and both scattering and absorption are at their highest levels (Manoharan et al., 2014; Dumka and Kaskaoutis, 2014). Hyvärinen et al. (2009) found lowest values of Aitken-to-Accumulation mode ratio during the pre- and post-monsoon seasons over central Indian Himalayas indicating largest influence of LRT, which was also justified by the highest particle number concentrations (as in the present study). In contrast, during the monsoon season, the Aitken-to-Accumulation mode ratio was higher due to more efficient removal of

accumulation mode by the rain-washout process, implying that the aerosols are of smaller size, less aged and mostly freshly emitted, thus explaining the highest SAE values during July-September. The lowest SAE in November is an indicator of the abundance of aged coarse aerosols, whereas the local primary emissions are mostly at the Aitken size, thus contributing to the much larger SAE for the $D_{1\mu m}$ particles and to the general increase in SAE during winter due to the influence of bio-fuel burning. Similar values of SAE, but with different annual pattern (maximum of 1.5±0.1 in January and minimum of 0.7 ± 0.1 in September), were found in Anantapur (Gopal et al., 2014) indicating significant difference in source apportionment, influence of local emissions and seasonal meteorological conditions between the GH region and the southern Indian peninsula.

The monthly variation of the spectral AAE exhibits similar pattern for both size groups with larger values at shorter wavelengths (Fig. 4). However, the wavelength dependence of the AAE strongly differentiates as a function of season and particle size. It is higher for $D_{10\mu m}$ particles and increases from monsoon to winter and pre-monsoon (for both particle groups), suggesting differences in the source regions and dominant aerosol type. The larger values and wavelength dependence of AAE correspond to enhanced contribution of dust and carbonaceous aerosols from biofuel burning, while values of AAE around 1 are characteristic of dominance of fossil-fuel combustion (Kirchstetter et al., 2004). The highest wavelength dependence of AAE in March is a fingerprint of the larger dust contribution either locally emitted or long-range transported. The AAE for the $D_{1\mu m}$ is found to be slightly larger (mean of 1.14 ± 0.18 at 0.47-0.60 µm) than that of $D_{10\mu m}$ (mean of 1.07 ± 0.20 at 0.47-0.60 µm), with a maximum during December-March (~1.3) and minimum during monsoon (~1.0). Monthly-mean AAE values in the range of 1.0 to 1.6 are reported for Mukteshwar, close to Nainital (Hyvärinen et al. 2009), which are larger during winter, similarly to our results (Fig. 4). A wide range (from 0.16 to 2.16, mean of 1.43 ± 0.41) in AAE values was also found by Andreae et al. (2002) indicative of very contrasting air masses and aerosol absorption efficiencies in arid Israel. The AAEs for $D_{1\mu m}$ and $D_{10\mu m}$ have shown a correlation coefficient of ~0.9 and most of the data points lie close to the 1-1 line (Manoharan et al., 2014), suggesting rather consistency in the aerosol source regions, and negligible effect of the particle size. In synopsis, the increase in both absorption and scattering coefficients during the last week of October and November due to enhanced biomass-burning activity over northwestern India is generally associated with a weaker wavelength dependence of both scattering (Fig. 3) and absorption (Fig. 4), suggesting an abundance of super-micron aerosols that absorb in the whole spectrum (Manoharan et al., 2014).

313 The monthly evolution of the spectral backscatter fraction (b) is shown in Fig. 5 for both particle
314 sizes. The results show that the b is strongly wavelength dependent, with larger values at longer
315 wavelengths (opposite to that found for σ_{sp} and σ_{ap}, SAE and AAE). The larger SAE that was
316 found in monsoon (Fig. 3) indicates particles of smaller size, which are associated with more
317 isentropic scattering and smaller b values. During post-monsoon and winter, the b increases
318 (except a small decrease in November) reaching its highest value in March suggesting more
319 irregular type of scattering and favoring of backscatter, which is characteristic of the dust
320 particles (Liu et al., 2008). The b is larger at longer wavelengths, especially for the $D_{1\mu m}$
321 particles, since the backscatter wavelength dependence is lower than that of total scattering (Fig.
322 2) and, therefore, the backscatter-to-total scattering ratio (b) is more enhanced at longer
323 wavelengths. Slight higher b values are found for the sub-micron particles over Nainital at 0.45
324 and 0.55 μm, which become significantly higher at 0.7 μm compared to those of $D_{10\mu m}$ (Fig. 5).
325 This is because the coarse particles favor the forward scattering (i.e. larger asymmetry factor and
326 smaller b) than the smaller particles. The b at 0.55 μm lies in the range 0.034-0.089 (0.027-
327 0.100) with higher values in March 0.080 ± 0.005 (0.092 ±0.006) and lower in August 0.054 ±
328 0.010 (0.058 ± 0.012) for $D_{10\mu m}$ ($D_{1\mu m}$). On average, the b values at 0.55 μm were found to be
329 0.067 ± 0.009 for $D_{10\mu m}$ and 0.073 ± 0.012 for $D_{1\mu m}$, which are much lower than those (0.13 ±
330 0.09) reported at Anantapur (Gopal et al., 2014), suggesting presence of more aged aerosols and
331 of larger size over Nainital. Backscatter ratio value of 0.13 was reported at the Negev desert,
332 Israel under continental pollution conditions (Formenti et al., 2001; Andreae et al., 2002), while
333 similar values (0.14 ± 0.02) were found for polluted air masses in the northwestern and eastern
334 United States (Anderson et al., 1999; Sheridan and Ogren, 1999). Previous studies (Carrico et al.,
335 2003; Doherty et al., 2005) have shown that the b values are higher for dust and biomass burning
336 aerosols, while they may be also sensitive to composition (organic content and particle size
337 distribution) of aerosol (Twardowski et al., 2001; Boss et al., 2004).
338
339 Figure 6 shows the temporal evolution of the σ_{sp} and σ_{ap} for the sub-micron ($D_{1\mu m}$) particles as
340 fraction of the respective efficiencies of $D_{10\mu m}$ (i.e. $D_{1\mu m}/D_{10\mu m}$). Both fractions are below 1,
341 especially for the scattering as was seen in Fig. 2, suggesting that the particles larger than 1 μm
342 contribute more to scattering and absorption. The decreasing trend with the wavelength for the
343 sub-micron scattering fraction implies more wavelength sensitivity compared to $D_{10\mu m}$, whereas
344 it becomes rather neutral for the absorption, suggesting that the spectral absorption is similar for
345 both $D_{1\mu m}$ and $D_{10\mu m}$. The sub-micron absorption fraction is higher than that of scattering
346 suggesting that the SSA would be higher for $D_{1\mu m}$, as justified (SSA for $D_{1\mu m}$ = 0.93, SSA for
347 $D_{10\mu m}$ = 0.91) in a previous study (Dumka and Kaskaoutis, 2014)).

Both absorption and scattering sub-micron fractions exhibit a similar pattern with higher values during July-August, which are decreasing in the post-monsoon, increase again in December-January and decrease in March. The larger SAE in monsoon (Fig. 3) implies abundance of fine aerosols (large Aitken-to-Accumulation ratio, Hyvärinen et al., 2009) leading to enhanced sub-micron scattering. The concurrent high values of sub-micron absorption fraction in July-August suggest that either $D_{1\mu m}$ particles are more absorbing than the rest of the year or $D_{10\mu m}$ would be less absorbing in monsoon. Sub-micron scattering and absorption are sensitive to the local anthropogenic emissions (at the Aitken size) during the monsoon and winter months, thus exhibiting higher fractions compared to the rest of the period. Except of the particle size and shape that mostly define the scattering processes, the aerosol chemical composition plays a vital role in the absorption efficiency. The carbonaceous aerosols were found to contribute about 25% of the total aerosol mass in Nainital (Ram et al., 2010), while the WSOC/OC (water soluble organic carbon/organic carbon) ratio (0.55 ± 0.15) was found to be larger than that over the IGP locations, suggesting enhanced contribution from secondary organic aerosols (mostly in the Aitken size). Concerning the coarse-mode particles, except of the LRT dust from the arid and semi-arid regions in southwestern Asia (see Fig. 9), dust particles may originate from local wind-blown dust, dust re-suspension due to road traffic or dust due to farming activities over the GH region (Raatikainen et al., 2014).

3.3. Diurnal cycle of aerosol properties

The monthly-mean diurnal evolutions of σ_{sp}, σ_{ap}, SAE and AAE are shown in Fig. 7 (a-d), respectively, for both $D_{1\mu m}$ and $D_{10\mu m}$. The σ_{sp} and σ_{ap} exhibit similar diurnal and seasonal patterns, with post-monsoon to winter (and March) highs and monsoon lows. Both maxima are observed in November due to significant influence of transported smoke from agricultural burning (Dumka and Kaskaoutis, 2014), while a slight decrease is observed in January. The particle size seems to play an important role in both processes, resulting in higher scattering and absorption for particles larger than 1 μm during periods of high aerosol loading. Similar annual variation of both σ_{sp} and σ_{ap} was reported at Mukteshwar (Hyvärinen et al. 2009). The slight lower December-January values were attributed to the confinement of the IGP polluted boundary layer below the site's altitude. Furthermore, synoptic-scale transport and changing air-mass origin affect the aerosol loading over the Himalayan sites (Xu et al., 2014; Bucci et al., 2014). The annual variation of the σ_{ap} seems to follow that of the BC mass fraction, which was found to be ~1% during monsoon and 7.6% during winter (Ram et al., 2010), associated with variation in σ_{ap} (at 0.678 μm) from 0.9 to 33.9 Mm^{-1}. However, no significant difference in σ_{ap} and σ_{sp} was

found between weekdays and weekends in contrast to Anantapur, where a 7.8% reduction in σ_{sp} was reported in weekends (Gopal et al., 2014). The factor that seems to contribute to the increase in σ_{sp} and σ_{ap} during noon to afternoon hours, is the slope up-stream of the polluted air masses coming from the IGP after deepening (> 2.5-3 km) of the PBL over the Ganges valley. Local-scale daily wind patterns, like valley wind cells, may also influence the diurnal patterns of spectral σ_{sp} and σ_{ap}; upslope winds are expected to increase the aerosol loading over the site, while downslope winds result in atmospheric cleansing. Afternoon-to-evening peaks in σ_{sp} and σ_{ap} were also reported at Mukteshwar during the post-monsoon and winter seasons, which were vanished during monsoon (Hyvärinen et al. 2009).

The seasonal pattern of SAE reveals larger values during monsoon, which can be explained by the rain washout of the coarser aerosols, and a secondary increase during December-January mostly associated with local emissions from biofuel combustion (morning and evening maxima). The diurnal variation observed in December-January is smoothed during the rest of the year for both particle groups. In contrast to SAE, the diurnal pattern of AAE exhibits significant variability during October – March, indicating dominance of different aerosol types and mixing processes. Higher AAE values (>1.3-1.4) are observed during night-to-early morning hours in the winter season, while during noontime the AAE goes down to 1-1.2. Peaks in AAE during the morning and evening hours were also found over Mukteshwar (Hyvärinen et al. 2009) suggesting influence of local biomass burning, i.e. burning of leaves and wood for heating, which did not contribute to the diurnal patterns of σ_{sp} and σ_{ap} (Fig. 7a, b), as they are mostly affected by the LRT from IGP. The diurnal pattern of AAE reveals the influence of different aerosol sources and combustion processes, i.e. local emissions from biofuel burning in the early morning and evening (high values of AAE) and transport of mostly aged aerosols from fossil-fuel combustion in IGP during noon to early afternoon (low values of AAE) (Bergstrom et al., 2007). In contrast, any diurnal pattern flattens out during monsoon, when the low AAE values (below 1) are associated with lowest σ_{ap}.

Raatikainen et al. (2014) noted that the air masses up to Himalayan sites in winter travel at higher altitudes than the maximum BLH (~1-1.5 km) over the IGP, thus not being able to carry significant amount of aerosol and pollutants. Such pollution transportation is very much favored during pre-monsoon when the BLH is at its maximum (>3-3.5 km) and the dilution of aerosols in the vertical favors their uplift to Himalayan foothills. Therefore, the role of the IGP to the aerosol concentrations over the Himalayas is strongly related to BLH and dynamics. Figure 8 summarizes the seasonal-mean diurnal variations of σ_{sp}, σ_{ap}, SAE and AAE for $D_{10\mu m}$ along with

that of BLH. The latter was obtained from HYSPLIT model in hourly basis using the Turbulent Kinetic Energy (TKE) profile method (Draxler et al., 2012), supposing that the BLH is assigned to the height at which TKE either decreases by a factor of two or to a value less than 0.21 (m^2/s^2). The BLH exhibits a pronounced diurnal variation in all seasons, especially in pre-monsoon (March), when it can reach up to 2.7 km at early-afternoon hours. During nighttime and early morning, the BLH is only few meters thus trapping aerosols and pollutants near the ground.

The diurnal variation of the σ_{sp} and σ_{ap} exhibits systematic increase during noon-to-early afternoon hours, coinciding well with the maximum BLH. In contrast, numerous papers (Ganguly et al., 2006; Beegum et al., 2009; Srivastava et al., 2012; Dumka et al., 2013; Pathak et al., 2013; Gopal et al., 2014, and many references therein) have shown increased pollutant (mostly emphasizing to BC) concentrations over Indian cities during early morning and evening hours due to lower BLH and trapping of pollutants near the ground and lower concentrations during noontime (maximum BLH) due to enhanced convection and dilution of pollutants. These diurnal patterns correspond mostly to urban environments and enhanced local emissions. The contrasting diurnal variation of σ_{sp} and σ_{ap} at Nainital suggests dominance of long-range transported aerosols from the Ganges Basin and west Asia, since the uplift is favored by the deeper mixing layer during noontime. Note also a small time lag between maximum in BLH and aerosol scattering/absorption that exists 1-2 hours later. In contrast, the diurnal variation is nearly vanished during monsoon due to rainy washout, which seems to smooth the effect of the LRT and constitutes the most effective scavenging factor that controls the aerosol loading and evolution. Prabha et al. (2012) revealed the removal of pollution from the IGP to higher atmospheric levels in association with dynamically forced updrafts. Their results showed that the valley pollution could be uplifted to heights above the haze layer, favored by the buoyancy generated due to thermal heating of the surface during noon-to-early afternoon hours. Similar diurnal patterns of BC and aerosol concentrations were found over other Himalayan sites, like Nepal Climate Observatory - Pyramid (NCO-P), Nepal, and Darjeeling, eastern Indian Himalayas (Marinori et al., 2010; Sarkar et al., 2014). In contrast, the diurnal pattern of SAE and AAE does not exhibit significant variations in all seasons, although the slight higher values observed during early morning suggesting local influence of fine and freshly-emitted aerosols.

3.4. The role of wind and LRT in aerosol properties

The diurnal and seasonal evolution of the aerosol properties over Nainital is a function of the emission sources, meteorological conditions (rainfall, wind pattern), BLD and LRT. In this respect, the variation in σ_{sp}, σ_{ap}, SAE and AAE is examined against the wind speed and direction

(Fig. 9). In general, the results show that the west/southwest flow enhances the scattering and absorption coefficients, while the north air masses are mostly clean. The air flow from southeast direction is mostly associated with the monsoon circulation, higher rainfall and lower aerosol concentrations; however, it was found that the concentrations from this sector are similar to those from southwest during the other seasons. Similar findings (lower values for both scattering and absorption associated with east/southeast directions) were found at Mukteshwar (Hyvarinen et al., 2009), while the highest values were found for western and southwestern sectors. The maximum σ_{sp} and σ_{ap} values are mostly associated with moderate winds (4-6 ms^{-1}), supporting the higher contribution of the transported aerosols at the observational site. In contrast, the accumulation of pollutants over the urban areas is favored by calm winds resulting in larger values of the σ_{sp} (almost double for wind speed < 0.5 m s^{-1} compared to wind speed > 3 m s^{-1}) at Anantapur (Gopal et al., 2014). The east flow carries smaller particles with SAE greater than 1.2, which can be up to 1.6-1.8 for certain air masses from southeast; in contrast, the northwest sector is associated with larger particles (much lower values of SAE). However, the AAE is not so much dependent on the wind direction, revealing larger influence by the local emissions as discussed in Fig. 7. The valley-breeze circulation was found to have a strong impact on the aerosol composition even at the high-altitude (5079 m) NCO-P site in the Everest area (Decesari et al., 2010) and, therefore, is considered as the major mechanism for the aerosol transport from the polluted IGP up to Himalayas. This was further supported by chemical analysis of the WIOC/EC ratios between Nainital and IGP (Ram and Sarin, 2010), which revealed aerosol of similar sources.

The whole analysis revealed that the BLD and LRT play the major role in the aerosol field and temporal evolution over Nainital in all seasons except monsoon, when the rain washout is the main process. The potential aerosol source regions are difficult to be defined by simple air-mass back trajectories or even trajectory clusters. Therefore, an advanced technique (Concentrated Weighted Trajectory, CWT), which is able to quantify the regional contribution of each of advection pathway to the measured aerosol variable (Seibert et al., 1994; Dumka et al., 2013) was performed by combining statistical analysis of back trajectories with the aerosol properties (σ_{sp}, σ_{ap}, SAE and AAE). The trajectories ending at 500 m over Nainital were weighted on the basis of the measured aerosol properties during their arrival and each grid cell is assigned a concentration obtained by averaging trajectory-associated concentrations that had crossed the grid cell (Fig. 10 a-d):

$$C_{ij} = \frac{1}{\sum_{l=1}^{M} \tau_{ijl}} \sum_{l=1}^{M} C_l \tau_{ijl} \quad (1)$$

where C_{ij} is the average weighted concentration in a grid cell (i, j), C_l the measured variable, τ_{ijk} the number of k^{th} trajectory endpoints in the (i, j) grid cell and M the total number of trajectory endpoints in (i, j) grid (Seibert et al., 1994). The CWT analysis reveals that the major sources that contribute to the large values of σ_{sp}, σ_{ap} are detected in the northwestern and central IGP, central and southern Pakistan, arid regions in southwest Asia and, especially for the σ_{ap} (Fig. 10b), eastern IGP, Bangladesh and Bay of Bengal (BoB). It should be noted that the trajectories from eastern directions mostly occur during monsoon, thus associated with lower σ_{sp} values (Fig. 10a) and higher SAE (Fig. 10c), while the arid regions in the west contribute to lower SAE values. Finally, the AAE plot (Fig. 10d) clearly differentiates the areas contributing to high values (southwest arid Asia) from those of moderate-to-low values (central-eastern IGP and BoB). The former regions contribute to seasonal dust and agricultural burning aerosols characterized by larger values of AAE compared to the dominance of anthropogenic and fossil-fuel burning mostly occurred in central-eastern IGP (Ram and Sarin, 2010).

Many studies (Eck et al., 2010; Russell et al., 2010; Giles et al., 2012; Vijayakumar et al., 2012; Vijayakumar and Devara, 2014) have suggested the use of correlations between the aerosol absorption and scattering properties for the discrimination of different aerosol types. In this respect, we correlate the SAE with AAE for the whole set of measurements for both $D_{1\mu m}$ and $D_{10\mu m}$ groups (Fig. 11). Such a graph is able to reveal the existence of different aerosols, since the wavelength dependence of scattering and absorption differentiates for the various types. As far as the scattering is concerned, the fine-mode aerosols (biomass burning, soot, urban/industrial emissions) exhibit higher values, while sea-salt and desert dust show lower values of SAE. The AAE is commonly used for aerosol characterization with values around 1 to correspond to vehicle exhausts or fossil fuel combustions, whereas the AAE values in excess of biomass burning or dust aerosol are around 2 or even more (Kirchstetter et al., 2004; Bergstrom et al., 2007). Using AERONET retrievals, Russell et al. (2010) found AAE values varying between 1.2 and 3.0 for dust, 0.75 and 1.3 for urban/industrial, and 1.2 and 2.0 for biomass burning. The range of these values seems to be significant and at the same magnitude (1.2 - 1.8) to those reported by Eck et al. (2010) for mixtures of dust, smoke and pollution. The current results reveal a rather well mixed atmosphere without clear identification of specific aerosol types, as

was found over Kanpur during pre-monsoon (TIGERZ campaign, Giles et al., 2011). The SAE and AAE are somewhat homogeneously distributed around the mean values of SAE (0.9-1.1) and AAE (1-1.2), while few cases present large values of SAE associated with AAE of 1.0-1.5 revealing the presence of carbonaceous aerosols of mixed fossil and biofuel combustions. The scatter plot of σ_{sp} vs. σ_{ap} showed a strong correlation suggesting covariance in the scattering and absorption properties. For a certain absorption value, the scattering of $D_{10\mu m}$ particles was larger than that of $D_{1\mu m}$ for σ_{sp} values above 200 Mm^{-1} indicating that for clean atmospheres the discrimination of the optical properties between super-micron and sub-micron aerosols is really difficult. Further analysis revealed a general decrease in SAE with increasing σ_{sp} suggesting an increase in size and ageing aerosol processes (condensation, coagulation) under more turbid atmospheres. These conditions are mostly related to LRT from northwestern IGP and southwest Asia transporting various types of aerosols via upslope flows within a deeper mixing layer.

4. Conclusions

A comprehensive analysis of several extensive and intensive properties (total scattering, backscattering, light absorption and their wavelength dependence) of near-surface aerosols was performed in the current study, aiming to investigate the temporal evolutions and influence of transported plumes and boundary-layer dynamics. The measurements via AMF were made in the framework of GVAX campaign during June 2011 - March 2012. More specifically, the light scattering and absorption measurements, using three wavelengths integrated Nephelometer and PSAP, were analyzed along with meteorological variables, mixing-layer height and air-mass back trajectories. The main findings of the study are summarized as follows:

1. The meteorological field exhibited a seasonal-changing pattern, which along with the boundary layer dynamics and the upslope valley winds control the temporal evolution and the aerosol characteristics at Nainital. The surface wind showed a clear dominance of the northwest (winter and pre-monsoon) and southeast (summer monsoon) directions.
2. The scattering and absorption coefficients showed higher values during November and March due to the significant influence of biomass-burning aerosols and dust mixed with anthropogenic pollution, respectively, and low values during monsoon due to rainy washout process.
3. The Ångström wavelength exponents of scattering (SAE) and absorption (AAE) exhibited a seasonal variation, with monsoon high for SAE and late winter-to-March high for AAE. The higher SAE values during monsoon may be related to rainy washout and the removal of the coarser aerosol particles, while a secondary increase of SAE during winter was associated with local emissions from bio-fuel combustion. The latter seems to have an effect in

increasing AAE values during the same period, while the higher AAE in March was associated with increased dust occurrence.

4. The particle size played a major role in the scattering coefficient and SAE, while its effect was much lesser in the absorption processes. Thus, the absorption fraction by the sub-micron particles (<1 μm) was about 0.9 of that of <10 μm particles, while the respective scattering fraction was only 0.6.
5. The diurnal variation of both scattering and absorption coefficients revealed a noon-to-early afternoon maximum, which was clearly defined during October to March, while it was vanished during monsoon. This suggests that the largest aerosol concentrations were mostly attributed to transported plumes from the IGP and southwest Asia and not to local emissions, while the rainy washout effect modulates the diurnal cycle. Furthermore, the diurnal patterns of SAE and AAE revealed slight higher values during early morning and evening hours due to larger influence of the local emissions, suggesting that these aerosols are finer and more absorbing in nature than the aged transported plumes.
6. The highest values for both scattering and absorption were mostly associated with moderate winds (3-5 ms^{-1}) and southwest air flow, suggesting strong influence of transported aerosols from northwestern India and arid southwest Asia, contributing to lower SAE values. The larger influence of the aged transported aerosol plumes controlled by the dynamics in mixing–layer height resulted in a rather well-mixed aerosol field over the site, whereas a specific aerosol type can be detected only in a few cases.

Acknowledgement

The authors gratefully acknowledge the NOAA Air Resources Laboratory (ARL) for the provision of the HYSPLIT transport and dispersion model and/or READY website (http://www.arl.noaa.gov/ready.html) used in this publication. We are grateful to the US Department of Energy for deploying the Atmospheric Radiation Measurements Climate Research Facility and to the technical staff for providing valuable data (http://www.archive.arm.gov/). This study is carried out under GVAX (https://www.arm.gov/sites/amf/pgh/) project in collaboration among the DoE, IISc, SPL, ISRO and ARIES. We would like to thank the participants (scientists and technical staff) of the campaign for valuable support. Thanks are also due to the Editor and anonymous reviewers for their insightful comments and valuable suggestions, which improved the scientific content and clarity of the paper.

References

Adhikary, B., Carmichael G. R., Tang Y., Leung L. R., Qian Y., Schauer J. J., Stone E. A., Ramanathan V., and Ramana M. V.: Characterization of the seasonal cycle of south Asian aerosols: A regional-scale modeling analysis, J. Geophys. Res., 112, D22S22, doi: 10.1029/2006JD008143, 2007.

Anderson, T. L. and Ogren, J. A.: Determining aerosol radiative properties using the TSI 3563 integrating Nephelometer, Aerosol Sci. Tech., 29, 57–69, 1998.

Anderson, T. L., Covert, D. S., Wheeler, J. D., Harris, J. M., Perry, K. D., Trost, B. E., Jaffe, D. J., and Ogren, J. A.: Aerosol Backscatter Fraction and Single Scattering Albedo: Measured values and uncertainties at a coastal station in the pacific North West, J. Geophys. Res., 104(D21), 793–807, 1999.

Andreae, T.W., Andreae, M.O., Ichoku, C., Maenhaut W., Jan, C., Karnieli, A. and Orlovsky, L.: Light scattering by dust and anthropogenic aerosol at a remote site in the Negev desert, Israel, J. Geophys. Res., 107(D2), 4008, doi: 10.1029/2001JD900252, 2002.

Andrews, E., Ogren, J.A., Bonasoni, P., Marinoni A., Cuevas E., Rodríguez S., Sun J. Y., Jaffe D. A., Fischer E.V., Baltensperger U., Weingartner E., Collaud Coen M., Sharma S., Macdonald A. M., Leaitch W. R., Lin N.-H., Laj P., Arsov T. Kalapov I., Jefferson A., Sheridan P.: Climatology of aerosol radiative properties in the free troposphere, Atmos. Res., 102, 365–393, doi:10.1016/j.atmosres.2011.08.017, 2011.

Antón, M., Valenzuela, A., Cazorla, A., et al.: Global and diffuse shortwave irradiance during a strong desert dust episode at Granada (Spain), Atmos. Res., 118, 232-239, doi: 10.1016/j.atmosres.2012.07.007, 2012.

Beegum S. Naseema, Moorthy K. Krishna, Babu S. Suresh, Satheesh S.K., Vinoj V., Badarinath K.V.S., Safai P.D., Devara P.C.S., Singh Sacchidanand, Vinod, Dumka U. C., Pant P.: Spatial distribution of aerosol black carbon over India during pre-monsoon Season, Atmos. Environ., 43, 1071–1078, doi:10.1016/j.atmosenv.2008.11.042, 2009.

Bergstrom, R. W., Pilewskie, P., Russell, P. B., Redemann, J., Bond, T. C., Quinn, P. K., and Sierau, B.: Spectral absorption properties of atmospheric aerosols, Atmos. Chem. Phys., 7, 5937–5943, 2007, http://www.atmos-chem-phys.net/7/5937/2007/.

Bollasina M., and Nigam S.: Absorbing aerosols and pre-summer monsoon hydroclimate variability over the Indian subcontinent: The challenge in investigating links, Atmos. Res., 94, 338–344, doi:10.1016/j.atmosres.2009.06.008, 2009.

Bond, T. C., Anderson, T. L., and Campbell, D.: Calibration and intercomparison of filter-based measurements of visible light absorption by aerosols, Aerosol Sci. Tech., 30, 582–600, 1999.

Bond, T. C.: Spectral dependence of visible light absorption by carbonaceous particles emitted from coal combustion, Geophys. Res. Lett., 28, 4075–4078, 2001.

Boss, E., Pegau W. S., Lee M., Twardowski M., Shybanov E., Korotaev G., and Baratange F.: Particulate backscattering ratio at LEO 15 and its use to study particle composition and distribution, J. Geophys. Res., 109, C01014, doi: 10.1029/2002JC001514, 2004.

Bucci, S., Cagnazzo C., Cairo F., Di Liberto L., and Fierli, F: Aerosol variability and atmospheric transport in the Himalayan region from CALIOP 2007–2010 observations, Atmos. Chem. Phys., 14, 4369–4381, doi:10.5194/acp-14-4369-2014, 2014.

Carrico, C. M., Kus P., Rood M. J., Quinn P. K., and Bates T. S.: Mixtures of pollution, dust, sea salt, and volcanic aerosol during ACE-Asia: Radiative properties as a function of relative humidity, J. Geophys. Res., 108(D23), 8650, doi: 10.1029/2003JD003405, 2003.

632 Decesari S, Facchini M.C, Carbone C, Giulianelli L, Rinaldi M, Finessi E, et al.: Chemical
633 composition of PM_{10} and PM_1 at the high-altitude Himalayan station Nepal Climate
634 Observatory-Pyramid (NCO-P) (5079 m a.s.l.), Atmos. Chem. Phys., 10, 4583-4596,
635 doi:10.5194/acp-10-4583-2010, 2010.
636 Di Girolamo, L., Bond T. C., Bramer D., Diner D. J., Fettinger F., Kahn R. A., Martonchik J. V.,
637 Ramana M. V., Ramanathan V., and Rasch P. J.: Analysis of Multi-angle Imaging
638 Spectroradiometer (MISR) aerosol optical depths over greater India during winter 2001–2004,
639 Geophys. Res. Lett., 31, L23115, doi: 10.1029/2004GL021273, 2004.
640 Dipu, S., Prabha Thara V., Pandithurai G., Dudhia J., Pfister G., Rajesh K., and Goswami B.N.:
641 Impact of elevated aerosol layer on the cloud macrophysical properties prior to monsoon
642 onset, Atmos. Environ., *70*, 454-467, 2013.
643 Doherty, S. J., Quinn P. K., Jefferson A., Carrico C. M., Anderson T. L. and Hegg D.: A
644 comparison and summary of aerosol optical properties as observed in situ from aircraft, ship,
645 and land during ACE-Asia, J. Geophys. Res., 110, D04201, doi: 10.1029/2004JD004964,
646 2005.
647 Draxler, R. et al.: HYSPLIT4 user's guide, version 4, report, NOAA, Silver Spring, Md.
648 [www.arl.noaa.gov/documents/reports/hysplit_user_guide.pdf], 2012.
649 Dumka U. C., Moorthy K Krishna, Satheesh S. K., Sagar Ram and Pant P.: Short-Period
650 Modulations in Aerosol Optical Depths over the Central Himalayas: Role of Mesoscale
651 Processes, J. Appl. Meteorol. Climatol, 47, 1467-1475, DOI: 10.1175/2007JAMC1638.1,
652 2008.
653 Dumka, U. C. and Kaskaoutis D. G.: In-situ measurements of aerosol properties and estimates of
654 radiative forcing efficiency over Gangetic-Himalayan region during the GVAX field
655 campaign, Atmos. Environ., 94, 96-105, 10.1016/j.atmosenv.2014.05.021, 2014.
656 Dumka, U. C., Satheesh S. K., Pant P., Hegde P. and Moorthy K. Krishna: Surface changes in
657 solar irradiance due to aerosols over central Himalayas, Geophys. Res. Lett., 33, L20809, doi:
658 10.1029/2006GL027814, 2006.
659 Dumka, U.C., Manchanda, R.K., Sinha, P.R., Sreenivasan, S., Moorthy, K.K., and Babu, S.S.:
660 Temporal variability and radiative impact of Black Carbon aerosol over tropical urban station
661 Hyderabad, J. Atmos. Sol-Terr. Phys., 105–106, 81-90, 2013.
662 Dumka, U.C., Moorthy K. K., Kumar, R., Hegde, P., Sagar, R., Pant, P., Singh, N., and Babu, S.
663 S.: Characteristics of aerosol black carbon mass concentration over a high altitude location in
664 the Central Himalayas from multi-year measurements, Atmos. Res., 96, 4, 510–521, ISSN
665 0169-8095, doi:10.1016/j.atmosres.2009.12.010, 2010.
666 Eck, T. F., Holben B. N., Sinyuk A., Pinker R. T., Goloub P., Chen H., Chatenet B., Li Z., Singh
667 R. P., Tripathi S. N., Reid J. S., Giles D. M., Dubovik O., O'Neill N. T., Smirnov A., Wang P.
668 and Xia X.: Climatological aspects of the optical properties of fine/coarse mode aerosol
669 mixtures, J. Geophys. Res., 115, D19205, doi: 10.1029/2010JD014002, 2010.
670 Fierz-Schmidhauser R., Zieger P., Gysel M., Kammermann L., DeCarlo P. F., Baltensperger U.,
671 and Weingartner E.: Measured and predicted aerosol light scattering enhancement factors at
672 the high alpine site Jungfraujoch, Atmos. Chem. Phys., 10, 2319–2333, 2010.
673 Formenti P., Andreae M. O., Andreae T. W., Ichoku C., Schebeske G., Kettle J., Maenhaut W.
674 Cafmeyer J., Ptasinsky J., Karnieli A. and Lelieveld J.: Physical and chemical characteristics
675 of aerosols over the Negev Desert (Israel) during summer 1996, J. Geophys. Res.,
676 106(D5), 4871-4890, 2001.

677 Ganguly, D., Jayaraman A., Rajesh T. A., and Gadhavi H: Wintertime aerosol properties during
678 foggy and non foggy days over urban center Delhi and their implications for shortwave
679 radiative forcing, J. Geophys. Res., 111, D15217, doi: 10.1029/2005JD007029, 2006.
680 Ganguly, D., Rasch P. J., Wang H., and Yoon J.H.: Climate response of the South Asian
681 monsoon system to anthropogenic aerosols. J. Geophys. Res., 117, D13209, doi:
682 10.1029/2012JD017508, 2012.
683 Gautam R., Hsu N. C., Tsay S. C., Lau K. M., Holben B., Bell S., Smirnov A., Li C., Hansell R.,
684 Ji Q., Payra S., Aryal D., Kayastha R. and Kim K. M.: Accumulation of aerosols over the
685 Indo-Gangetic plains and southern slopes of the Himalayas: distribution, properties and
686 radiative effects during the 2009 pre-monsoon season, Atmos. Chem. Phys., 11, 12841–
687 12863, doi: 10.5194/acp-11-12841-2011, 2011.
688 Gautam, R., Hsu, N. C., and Lau, K.-M.: Premonsoon aerosol characterization and radiative
689 effects over the Indo-Gangetic Plains: Implications for regional climate warming, J. Geophys.
690 Res., 115, D17208, doi: 10.1029/2010JD013819, 2010.
691 Giles DM, Holben BN, Tripathi SN, Eck T, Newcomb W, Slutsker I, Dickerson R, Thompson A,
692 Mattoo S, Wang S, Singh R, Sinyuk A, Schafer J (2011). Aerosol Properties over the Indo-
693 Gangetic Plain: A 1 Mesoscale Perspective from the TIGERZ Experiment. J Geophys Res
694 116: D18203, doi: 10.1029/2011JD015809
695 Giles, D. M., Holben B. N., Eck T. F., Sinyuk A., Smirnov A., Slutsker I., Dickerson R. R.,
696 Thompson A. M., and Schafer J. S.: An analysis of AERONET aerosol absorption properties
697 and classifications representative of aerosol source regions, J. Geophys. Res., 117, D17203,
698 doi: 10.1029/2012JD018127, 2012.
699 Gopal K. Rama, Arafath S. Md., Lingaswamy A.P., Balakrishnaiah G., Kumari S. Pavan, Uma
700 Devi K., Reddy N. Siva Kumar, Reddy K. Raja Obul, Reddya M. Penchal, Reddy R.R., Babu
701 S. Suresh: In-situ measurements of atmospheric aerosols by using Integrating Nephelometer
702 over a semi-arid station, southern India, Atmos. Environ., 86, 228-240, 2014.
703 Guleria Raj Paul, Kuniyal Jagdish Chandra, Rawat Pan Singh, Sharma Nand Lal, Thakur
704 Harinder Kumar, Dhyani Pitamber Prasad and Singh Mahavir: The assessment of aerosol
705 optical properties over Mohal in the northwestern Indian Himalayas using satellite and
706 ground-based measurements and an influence of aerosol transport on aerosol radiative
707 forcing, Meteorol Atmos Phys, 113, 153-169, DOI 10.1007/s00703-011-0149-5, 2011.
708 Hegde P. and Kawamura K.: Seasonal variations of water-soluble organic carbon, dicarboxylic
709 acids, ketocarboxylic acids, and α-dicarbonyls in Central Himalayan aerosols, Atmos. Chem.
710 Phys., 12, 6645–6665, doi: 10.5194/acp-12-6645-2012, 2012.
711 Hegde, P., Pant, P., Naja, M., Dumka, U. C., and Sagar, R.: South Asian dust episode in June
712 2006: Aerosol observations in the central Himalayas, Geophys. Res. Lett., 34, L23802, doi:
713 10.1029/2007GL030692, 2007.
714 Heintzenberg, J., Wiedensohler, A., Tuch, T. M., Covert, D. S., Sheridan, P., Ogren, J. A., Gras,
715 J., Nessler, R., Kleefeld, C., Kalivitis, N., Aaltonen V., Wilhelm, R. T., and Havlicek, M.:
716 Intercomparison and aerosol calibrations of 12 commercial integrating Nephelometer of three
717 manufacturers, J. Atmos. Ocean. Tech., 23, 902–914, 2006.
718 Hyvärinen A.-P., Raatikainen T., Brus D., Komppula M., Panwar T. S., Hooda R. K., Sharma V.
719 P., and Lihavainen H.: Effect of the summer monsoon on aerosols at two measurements
720 stations in Northern India – Part 1: PM and BC concentrations, Atmos. Chem. Phys., 11,
721 8271–8282, doi:10.5194/acp-11-8271-2011, 2011a.

722 Hyvärinen A.-P., Raatikainen T., Komppula M., Mielonen T., Sundström A.-M., Brus D.,
723 Panwar T. S., Hooda R. K., Sharma V. P., de Leeuw G., and Lihavainen H.: Effect of the
724 summer monsoon on aerosols at two measurement stations in Northern India – Part 2:
725 Physical and optical properties, Atmos. Chem. Phys., 11, 8283–8294, doi: 10.5194/acp-11-
726 8283-2011, 2011b.
727 Hyvärinen, A.-P, Lihavainen, H., Komppula, M., Sharma, V. P., Kerminen, V.-M., Panwar, T.
728 S., and Viisanen, Y.: Continuous measurements of optical properties of atmospheric aerosols
729 in Mukteshwar, Northern India, J. Geophys. Res., 114, D08207, doi: 10.1029/2008JD011489,
730 2009.
731 Jayaraman A., Gadhavi H., Misra A., Ganguly D., Ramachandran S. and Rajesh T.A.: Spatial
732 variations in aerosol characteristics and regional radiative forcing over India: Measurements
733 and modeling of 2004 road campaign experiment, Atmos. Environ., 40, 6504–6515,
734 doi:10.1016/j.atmosenv.2006.01.034, 2006.
735 Jefferson A.: Aerosol Observing System (AOS) Handbook, DOE/SC-ARM/TR-014,
736 [http://www.arm.gov/publications/tech_reports/handbooks/aos_handbook.pdf], 2011.
737 Kaskaoutis D. G., Singh Ramesh P, Gautam Ritesh, Sharma Manish, Kosmopoulos P G and
738 Tripathi S N.: Variability and trends of aerosol properties over Kanpur, northern India using
739 AERONET data (2001-10), Environ. Res. Lett., 7, 024003, doi:10.1088/1748-
740 9326/7/2/024003, 2012.
741 Kaskaoutis D.G., Kumar S., Sharma D., Singh R.P., Kharol S.K., Sharma M., Singh A.K., Singh
742 S., Singh Atinderpal and Singh D.: Effects of crop residue burning on aerosol properties,
743 plume characteristics and longrange transport over northern India, J. Geophys. Res., doi:
744 10.1002/ 2013JD021357, 2014.
745 Kaskaoutis D.G., Sinha P.R., Vinoj V., Kosmopoulos P. G., Tripathi S. N., Misra Amit, Sharmaf
746 M., Singh R. P.: Aerosol properties and radiative forcing over Kanpur during severe aerosol
747 loading conditions, Atmos. Environ., 79, 7-19, doi:10.1016/j.atmosenv.2013.06.020, 2013.
748 Kirchstetter, T. W., Novakov T., and Hobbs P. V.: Evidence that the spectral dependence of light
749 absorption by aerosols is affected by organic carbon, J. Geophys. Res., 109, D21208, doi:
750 10.1029/2004JD004999, 2004.
751 Komppula, M., Lihavainen, H., Hyvärinen, A.-P., Kerminen, V.-M., Panwar, T. S., Sharma, V.
752 P., and Viisanen, Y.: Physical properties of aerosol particles at a Himalayan background site
753 in India, J. Geophys. Res., 114, D12202, doi: 10.1029/2008JD011007, 2009.
754 Kopacz, M., Jacob, D. J., Fisher, J. A., Logan, J. A., Zhang, L., Megretskaia, I. A., Yantosca, R.
755 M., Singh, K., Henze, D. K., Burrows, J. P., Buchwitz, M., Khlystova, I., McMillan, W. W.,
756 Gille, J. C., Edwards, D. P., Eldering, A., Thouret, V., and Nedelec, P.: Global estimates of
757 CO sources with high resolution by adjoint inversion of multiple satellite datasets (MOPITT,
758 AIRS, SCIAMACHY, TES), Atmos. Chem. Phys., 10, 855–876, doi:10.5194/acp-10-855-
759 2010, 2010.
760 Kotamarthi, V. R. and Satheesh S. K.: Ganges Valley Aerosol Experiment, Air & Waste
761 Management Association, Em, The magazine for environmental managers, 2011.
762 Kumar, R., Barth M. C., Pfister G. G., Naja M. and Brasseur G. P.: WRF-Chem simulations of a
763 typical pre-monsoon dust storm in northern India: influences on aerosol optical properties and
764 radiation budget, Atmos. Chem. Phys., 14, 2431–2446, doi: 10.5194/acp-14-2431-2014, 2014.

765 Lau K M, Kim M K, Kim K M.: Asian summer monsoon anomalies induced by aerosol direct
766 forcing: the role of the Tibetan Plateau, Clim Dyn., 26, 855–864, DOI 10.1007/s00382-014-
767 2055-2, 2006.
768 Lawrence, M. G. and Lelieveld, J.: Atmospheric pollutant outflow from Southern Asia: a review,
769 Atmos. Chem. Phys., 10, 11017-11096, doi: 10.5194/acp-10-11017-2010, 2010.
770 León, J.-F., and Legrand M.: Mineral dust sources in the surroundings of the north Indian Ocean,
771 Geophys. Res. Lett., 30(6), 1309, doi: 10.1029/2002GL016690, 2003.
772 Liu Z., Liu D., Huang J., Vaughan M., Uno I., Sugimoto N., Kittaka C., Trepte C., Wang Z.,
773 Hostetler C., and Winker D.: Airborne dust distributions over the Tibetan Plateau and
774 surrounding areas derived from the first year of CALIPSO lidar observations, Atmos. Chem.
775 Phys., 8, 5045–5060, 2008.
776 Lu, Z, Zhang Q., and Streets D.G.: Sulfur dioxide and primary carbonaceous aerosol emissions
777 in China and India, 1996–2010, Atmos. Chem. Phys., 11, 9839-9864, doi: 10.5194/acp-11-
778 9839-2011, 2011.
779 Manoharan V. S., Kotamarthi R., Feng Y., and Cadeddu M. P.: Increased absorption by coarse
780 aerosol particles over the Gangetic–Himalayan region, Atmos. Chem. Phys., 14, 1159–1165,
781 doi: 10.5194/acp-14-1159-2014, 2014.
782 Manoj M. G., Devara, P. C. S., Safai P. D., and Goswami B. N.: Absorbing aerosols facilitate
783 transition of Indian monsoon breaks to active spells, Clim Dyn 37, 2181-2198, 2011.
784 Marcq, S., Laj, P., Roger, J. C., Villani, P., Sellegri, K., Bonasoni, P., Marinoni, A., Cristofanelli,
785 P., Verza, G. P., and Bergin, M.: Aerosol optical properties and radiative forcing in the high
786 Himalaya based on measurements at the Nepal Climate Observatory-Pyramid site (5079 m
787 a.s.l.), Atmos. Chem. Phys., 10, 5859–5872, doi:10.5194/acp-10-5859-2010, 2010.
788 Marinoni, A., Cristofanelli, P., Laj, P., Duchi, R., Calzolari, F., Decesari, S., et al.: Aerosol mass
789 and black carbon concentrations, a two year record at NCO-P (5079 m, Southern Himalayas),
790 Atmos. Chem. Phys., 10, 8551-8562, doi: 10.5194/acp-10-8551-2010, 2010.
791 Nakajima, T., Yoon, S.-C., Ramanathan, V., Shi, G.-Y., Takemura, T., Higurashi, A., Takamura,
792 T., Aoki, K., Sohn, B.-J., Kim, S.-W., Tsuruta, H., Sugimoto, N., Shimizu, A. Tanimoto, H.,
793 Sawa, Y., Lin, N.-H., Lee, C.-T., Goto, D., and Schutgens, N.: Overview of the atmospheric
794 Brown Cloud East Asian Regional Experiment 2005 and a study of the aerosol direct radiative
795 forcing in east Asia, J. Geophys. Res., 112, D24S91, doi: 10.1029/2007JD009009, 2007.
796 Neitola K., Asmi E., Komppula M., Hyvärinen A.-P. Raatikainen T., Panwar T. S., Sharma V. P.
797 and Lihavainen H.: New particle formation infrequently observed in Himalayan foothills –
798 why?, Atmos. Chem. Phys., 11, 8447–8458, doi: 10.5194/acp-11-8447-2011, 2011.
799 Ogren, J.A.: Comment on "Calibration and Intercomparison of Filter-Based Measurements of
800 Visible Light Absorption by Aerosols", Aerosol Sci. Tech., 44, 589–591, 2010.
801 Pant, P., Hegde, P., Dumka, U. C., Sagar, R., Satheesh, S. K., Moorthy, K. K., Saha, A., and
802 Srivastava, M. K.: Aerosol characteristics at a high-altitude location in central Himalayas:
803 Optical properties and radiative forcing, J. Geophys. Res., 111, D17206, doi:
804 10.1029/2005JD006768, 2006.
805 Panwar T. S., Hooda Rakesh K., Lihavainen H., Hyvärinen A. P., Sharma V. P., Viisanen Y.:
806 Atmospheric aerosols at a regional background Himalayan site-Mukteshwar, India, Environ
807 Monit Assess, 185:4753–4764, DOI 10.1007/s10661-012-2902-8, 2013.

808 Pathak, B., Bhuyan, P.K., Biswas, J., and Takemura, T.: Long term climatology of Particulate
809 Matter and associated microphysical and optical properties over Dibrugarh, North-East India
810 and inter-comparison with SPRINTARS simulations, Atmos. Environ., 69, 334-344, 2013.
811 Prabha T. V., Karipot, A., Axisa D., Padmakumari B., Maheskumar R. S., Konwar M., Kulkarni
812 J. R., Goswami B. N.: Scale interactions near the foothills of Himalaya during CAIPEEX, J.
813 Geophys. Res., 117, D10203, 495 doi: 10.1029/2011JD0167, 2012.
814 Raatikainen T., Hyvärinen A.-P., Hatakka J., Panwar T.S., Hooda R.K., Sharma V.P., Lihavainen
815 H.: The effect of boundary layer dynamics on aerosol properties at the Indo-Gangetic plains
816 and at the foothills of the Himalayas, Atmos. Environ., 89, 548-555,
817 http://dx.doi.org/10.1016/j.atmosenv.2014.02.058, 2014.
818 Ram Kirpa and Sarin M. M: Spatio-temporal variability in atmospheric abundances of EC, OC
819 and WSOC over Northern India, J. Aer. Sci., 41(1), 88-98,
820 doi:10.1016/j.jaerosci.2009.11.004, 2010.
821 Ram, K., Sarin, M. M., and Hedge, P.: Atmospheric abundances of primary and secondary
822 carbonaceous species at two high-altitude sites in India: Sources and temporal variability,
823 Atmos. Environ., 42(28), 6785–6796, 2008.
824 Ram, K., Sarin, M. M., and Tripathi, S. N.: A 1 year record of carbonaceous aerosols from an
825 urban site in the Indo-Gangetic Plain: Characterization, sources, and temporal variability, J.
826 Geophys. Res., 115, D24313, doi: 10.1029/2010JD014188, 2010.
827 Ramanathan, V., Chung, C., Kim, D., Bettge, T., Buja, L., Kiehl, J.T., Washington, W.M., Fu,
828 Q., Sikka, D.R., Wild, M.: Atmospheric brown clouds: impacts on South Asian climate and
829 hydrological cycle. PNAS 102 (15), 5326-5333. http://dx.doi.org/10.1073/pnas.0500656102,
830 2005.
831 Ramanathan, V., Li F., Ramana M. V., Praveen P. S., Kim D., Corrigan C. E., Nguyen H., Stone
832 Elizabeth A., Schauer James J., Carmichael, G. R. Adhikary Bhupesh, and Yoon S. C.:
833 Atmospheric brown clouds: Hemispherical and regional variations in long-range transport,
834 absorption, and radiative forcing, J. Geophys. Res., 112, D22S21, doi:
835 10.1029/2006JD008124, 2007.
836 Randles, C. A. and Ramaswamy, V.: Absorbing aerosols over Asia: A Geophysical Fluid
837 Dynamics Laboratory general circulation model sensitivity study of model response to aerosol
838 optical depth and aerosol absorption, J. Geophys. Res., 113, D21203, doi:
839 10.1029/2008JD010140, 2008.
840 Russell, P. B., Bergstrom R. W., Shinozuka Y., Clarke A. D., DeCarlo P. F., Jimenez J. L.,
841 Livingston J. M., Redemann J., Dubovik O., and Strawa A.: Absorption Ångström Exponent
842 in AERONET and related data as an indicator of aerosol composition, Atmos. Chem. Phys.,
843 10, 1155–1169, doi:10.5194/acp-10-1155-2010, 2010.
844 Sarkar, C., Chatterjee, A., Singh, A.K., Ghosh, S.K., and Raha, S.: Characterization of Black
845 Carbon aerosols over Darjeeling - A high altitude Himalayan station in Eastern India, Aeros.
846 Air Qual. Res., (in press), doi: 10.4209/aaqr.2014.02.0028, 2014.
847 Seibert P, et al.: Trajectory analysis of aerosol measurements at high alpine sites, in Transport
848 and Transformation of Pollutants in the Troposphere: Proceedings of EUROTRAC
849 Symposium ’94. Edited by Borrell PM Cvitas T, Seiler W, pp. 689– 693, SPB Acad. Publ.,
850 Hague, The Netherlands, 1994.

Sheridan, P. J. and Ogren, J. A.: Observations of the vertical and regional variability of aerosol optical properties over central and eastern North America, J. Geophys. Res., 104, 16793–16805, doi: 10.1029/1999JD900241, 1999.

Sheridan, P. J., Delene, D. J., and Ogren, J. A.: Four years of continuous surface aerosol measurements from the Department of Energy's Atmospheric Radiation Measurement Program Southern Great Plains Cloud and Radiation Testbed site, J. Geophys. Res., 106, 20735–20747, doi: 10.1029/2001JD000785, 2001.

Srivastava, A.K., Singh, S., Pant, P., and Dumka, U.C.: Characteristics of Black Carbon over Delhi and Manora Peak – a comparative study, Atmos. Sci. Lett. 13, 223-230, 2012.

Titos, G., Jefferson, A., Sheridan, P. J., Andrews, E., Lyamani, H., Alados-Arboledas L., and Ogren J. A.: Aerosol light-scattering enhancement due to water uptake during TCAP campaign, Atmos. Chem. Phys., 14, 7031–7043, doi: 10.5194/acp-14-7031-2014, 2014a.

Titos, G., Lyamani, H., Cazorla, A., Sorribas, M., Foyo-Moreno, I., Wiedensohler, A. and Alados-Arboledas, L.: Study of the relative humidity dependence of aerosol light-scattering in southern Spain, Tellus B, 66, 24536, http://dx.doi.org/10.3402/tellusb.v66.24536, 2014b.

Twardowski Michael S., Boss Emmanuel, Macdonald Jacob B., Pegau W. Scott, Barnard Andrew H., and Zaneveld J. Ronald V.: A model for estimating bulk refractive index from the optical backscattering ratio and the implications for understanding particle composition in case I and case II waters, J. Geophys. Res., 106, 14,129-14,142, 2001.

Vijayakumar, K. and Devara P.C.S.: Influence of aerosol type, fine- and coarse-mode fractions on regional monsoon activity, Proc. INTROMET, 07-10 January 2014, Kattankulathur, 2014.

Vijayakumar, K., Devara P.C.S., and Simha, C.P.: Aerosol features during drought and normal monsoon years: A study undertaken with multi-platform measurements over a tropical urban site, Aero. Air Qual. Res., 12, 1444-1458, 2012.

Virkkula A., Backman J., Aalto P. P., Hulkkonen M., Riuttanen L., Nieminen T., dal Maso M., Sogacheva L., de Leeuw G., and Kulmala M.: Seasonal cycle, size dependencies, and source analyses of aerosol optical properties at the SMEAR II measurement station in Hyytiälä, Finland, Atmos. Chem. Phys., 11, 4445–4468, doi:10.5194/acp-11-4445-2011, 2011.

Xu, C., Ma Y. M., Pandey A., Cong Z. Y., Yang K., Zhu Z. K., Wang J. M., Amatya P. M., and Zhao L: Similarities and differences of aerosol optical properties between southern and northern slopes of the Himalayas, Atmos. Chem. Phys., 14, 3133–3149, doi: 10.5194/acp-14-3133-2014, 2014.

884 **Table 1:** Details of AOS instruments, variables and equations used for the calculation of aerosol optical properties.

Instruments	Primary measurements	Derived variables	Equation
Three wavelength Nephelometer (TSI Model 3563)	Total scattering and hemispheric backscattering coefficients (σ_{sp} & σ_{bsp}) from D_1 and D_{10} particles at blue (0.45), green (0.55) and red (0.70) µm	Hemispheric backscatter fraction Scattering Ångström exponent Backscattering Ångström exponent Submicron scattering fraction	$b = \sigma_{bsp}/\sigma_{sp}$ $SAE = -\log[\sigma_{sp}(\lambda_1)/ \sigma_{sp}(\lambda_2)]/\log[\lambda_1/\lambda_2]$ $BAE= -\log[\sigma_{bsp}(\lambda_1)/\sigma_{bsp}(\lambda_2)]/\log[\lambda_1/\lambda_2]$ $R_{sp} = \sigma_{sp}(D_1)/\sigma_{sp}(D_{10})$
Radiance Research Particle Soot Absorption Photometer (PSAP)	Light absorption coefficient (σ_{ap}) from D_1 and D_{10} particles at blue (0.467), green (0.53) and red (0.66) µm	Absorption Ångström exponent Submicron absorption fraction	$AAE = -\log[\sigma_{ap}(\lambda_1)/ \sigma_{ap}(\lambda_2)]/\log[\lambda_1/\lambda_2]$ $R_{ap} = \sigma_{ap}(D_1)/\sigma_{ap}(D_{10})$

885
886
887
888
889
890
891
892
893
894
895
896

Table 2: Comparison of extensive and intensive aerosol properties over Nainital during GVAX campaign along with those measured over mountainous or remote areas over the globe.

Sampling Site	Elevation (m)	Sampling Period	σ_{sp} (Mm^{-1})	σ_{ap} (Mm^{-1})	SAE	AAE	Reference
Nainital	1958	Jun-11 to Mar-12	177.20 (104.40)*	10.90 (8.95)*	0.71 (1.21)*	1.07 (1.14)*	Present study
Nainital	1958	Feb-05 to Jul 08	--	13.9	--	--	Ram et al. (2010)
Nainital	1958	Dec-04	--	12.9	--	--	Ram and Sarin (2009)
Nainital	1958	Feb-05 to Jun-07	--	12.2	--	--	Ram and Sarin (2009)
Mukteshwar	2180	Sep-05 – Sep -07	53.00	11.00	--	1.0 to 1.6	Hyvärinen et al. (2009)
Mukteshwar	2180	2006 to 2009	34.30 – 133.80	6.90 – 25.8	--	--	Hyvärinen et al. (2011b)
NCO-P	5079	May-Sep-6	--	1.1	--	--	Marcq et al. (2010)
Mt. Abu	1700	Dec-05 to Feb-06	--	8.0	--	--	Ram and Sarin (2009)
Mt. Abu	1700	May-05 to Feb-06	--	5.8	--	--	Ram and Sarin (2009)
Cape Cod, MA	20	Jul 2012-Jul 2013	22 ± 15	1.1 ± 0.9	1.8 ± 0.6	--	Titos et al. (2014a)
Granada, Spain	680	Winter 2013	41 ± 34	17 ± 17	1.8 ± 0.4	--	Titos et al. (2014b)
		Spring 2013	38 ± 26	11 ± 11	1.8 ± 0.3		
Jungfraujoch	3580	May 2008**	1.19	--	--	--	Fierz-Schmidhauser et al. (2010)
		May 2008***	2.05	--	--	--	Fierz-Schmidhauser et al. (2010)

Mauna Loa, USA	3400	[a]2000-2009	1.92(1.24)	0.07(0.07)	1.53(1.35)	--	Andrews et al. (2011)
Whistler Canada	2200	[b]2008-2009	3.98(3.95)	0.54(0.53)	2.01(2.01)	--	Andrews et al. (2011)
Mount Bachelor, USA	2800	[c]April-May, 2008-2009	5.32(3.50)	1.00(0.77)	2.54(2.50)	--	Andrews et al. (2011)
Southern Great Plains		[d]2000-2007	13.00(5.73)	0.77(0.49)	2.09(1.89)	--	Andrews et al. (2011)
Bondville		[d]2006-2009	15.30(4.89)	1.00(0.31)	1.91(1.38)	--	Andrews et al. (2011)
Lzana Spain	2400	[a]2008-2009	9.32(6.57)	0.71(0.43)	0.73(0.63)	--	Andrews et al. (2011)
Jungfraujoch, Switzerland	3600	[e]1995-2007	3.50(5.87)	0.50(0.42)	1.85(1.75)	--	Andrews et al. (2011)
Monte Cimone, Italy	2200	[e]2007-2009	17.20(14.30)	2.45(2.00)		--	Andrews et al. (2011)
Moussala Peak, Bulgaria	2400	[e]2007-2009	16.00(12.20)		2.20(2.12)	--	Andrews et al. (2011)
NCO-P	5100	[f]2006-2008	17.40(10.70)	1.63(0.97)	1.59(1.22)	--	Andrews et al. (2011)
Mount Waliguan China	3800	[a]2005-2008	42.50(39.70)	2.31(1.94)	0.89(0.85)	--	Andrews et al. (2011)
Lulin Mountain, Tiwan	2900	[a]2008-2009	25.80(10.80)	2.83(0.97)	1.57(1.51)	--	Andrews et al. (2011)

***** Value inside parenthesis represents for $D_{1\mu m}$ size aerosols

**Value Excluding Saharan dust event (SDE)

*** Value Exclusively for Saharan dust event (SDE)

[a]Size cut (10 μm); [b]Size cut (2.5 μm); [c]Size cut (1.0 μm); [d]Size cut (7.0 μm); [e] Whole air; [f]Size cut (2.5 μm for scattering) and Size cut (10.0 μm for absorption)

Values taken from Andrews et al. (2011) are in STP and value inside the bracket represents for free troposphere

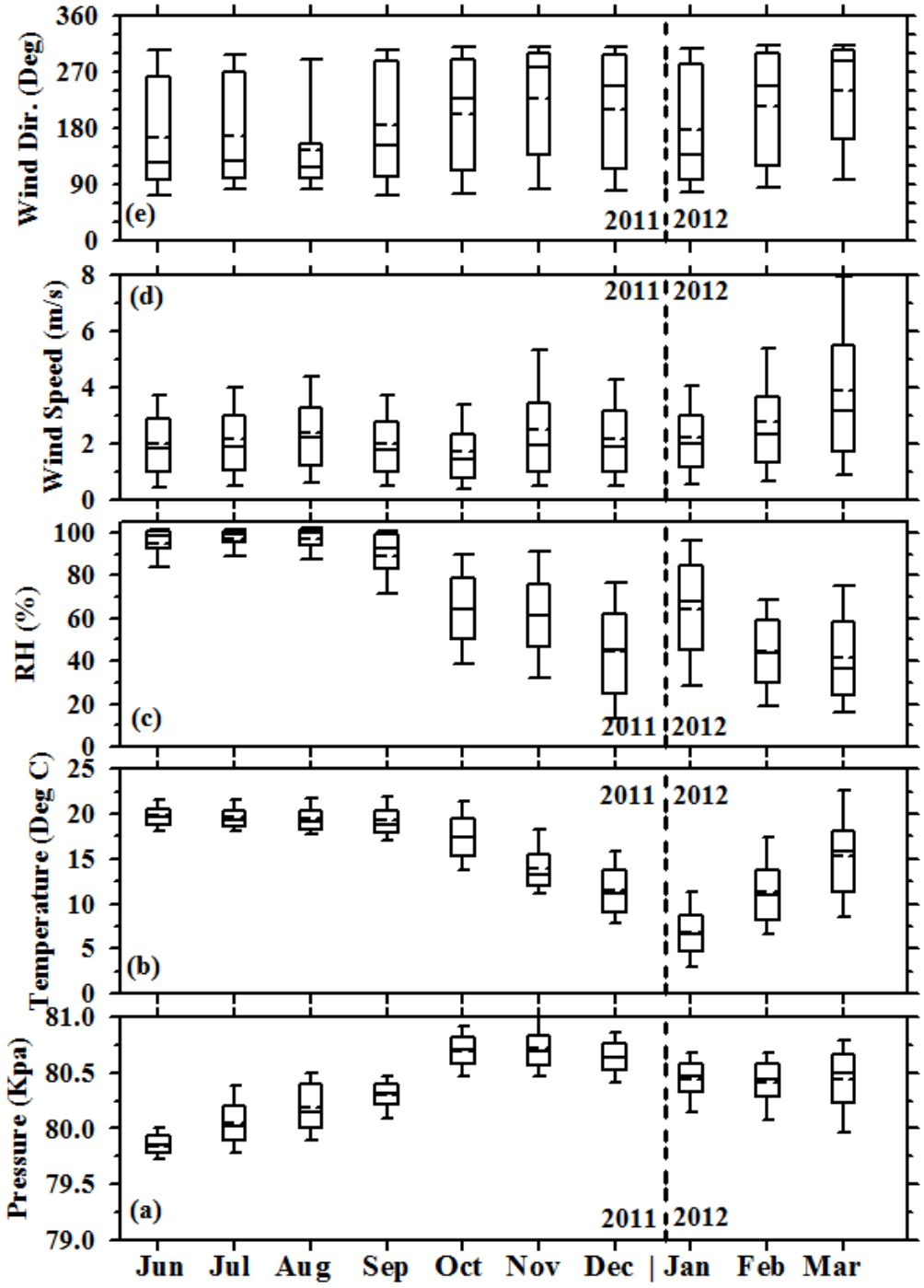

Figure 1: Monthly surface meteorological variables (ambient pressure, air Temperature, Relative Humidity, wind speed and direction) at Nainital during the period June 2011 to March 2012 in box and whisker charts. The dashed line represents the mean and the solid line the median. The box contains the range of values from 25% (bottom) to 75% (top).

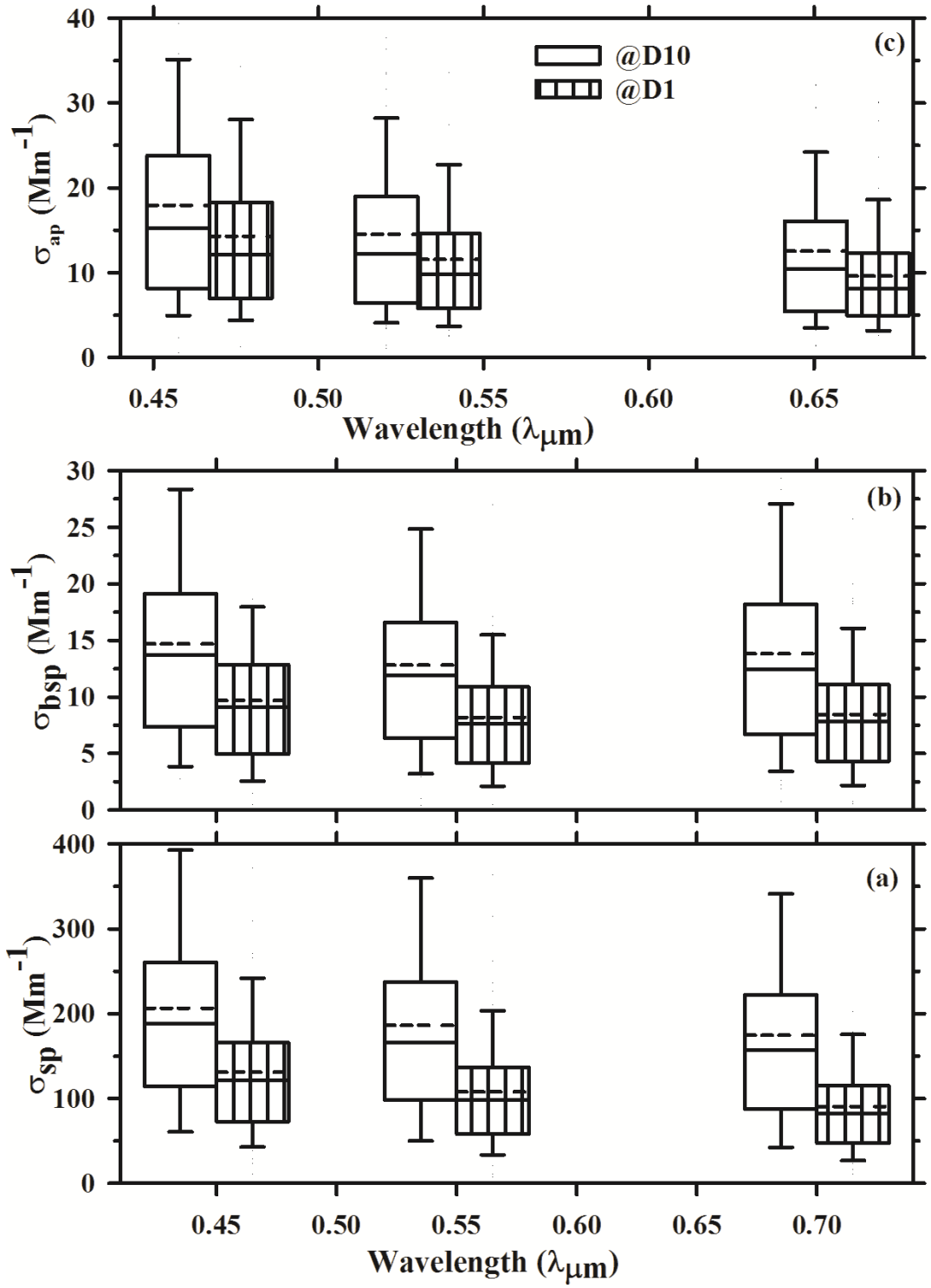

910

911 **Figure 2:** Statistical (box and whisker chart view) spectral distribution of (a) scattering
912 coefficient (σ_{sp}), (b) back scattering coefficient (σ_{bsp}) and, (c) absorption coefficient (σ_{ap}) at
913 Nainital during June 2011 – March 2012.

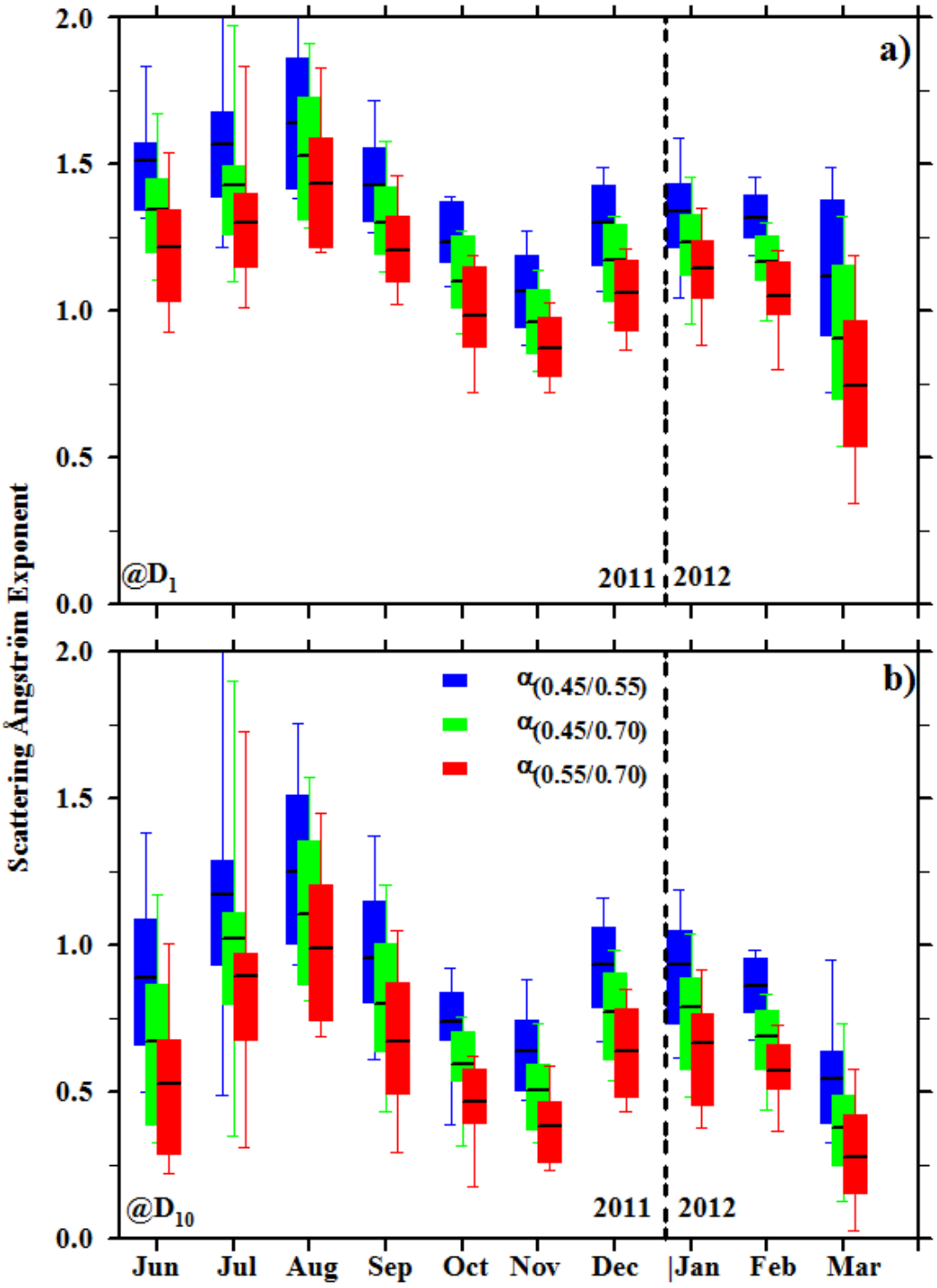

Figure 3: Monthly-mean variation of scattering Ångström exponent for $D_{1\mu m}$ (a) and $D_{10\mu m}$ (b) during June 2011 to March 2012. The box and whiskers denote the 95th and 5th percentiles, respectively. The box's upper and lower limits are 75th and 25th percentiles and black straight line shows the mean value. The vertical dotted line separates the years 2011 and 2012.

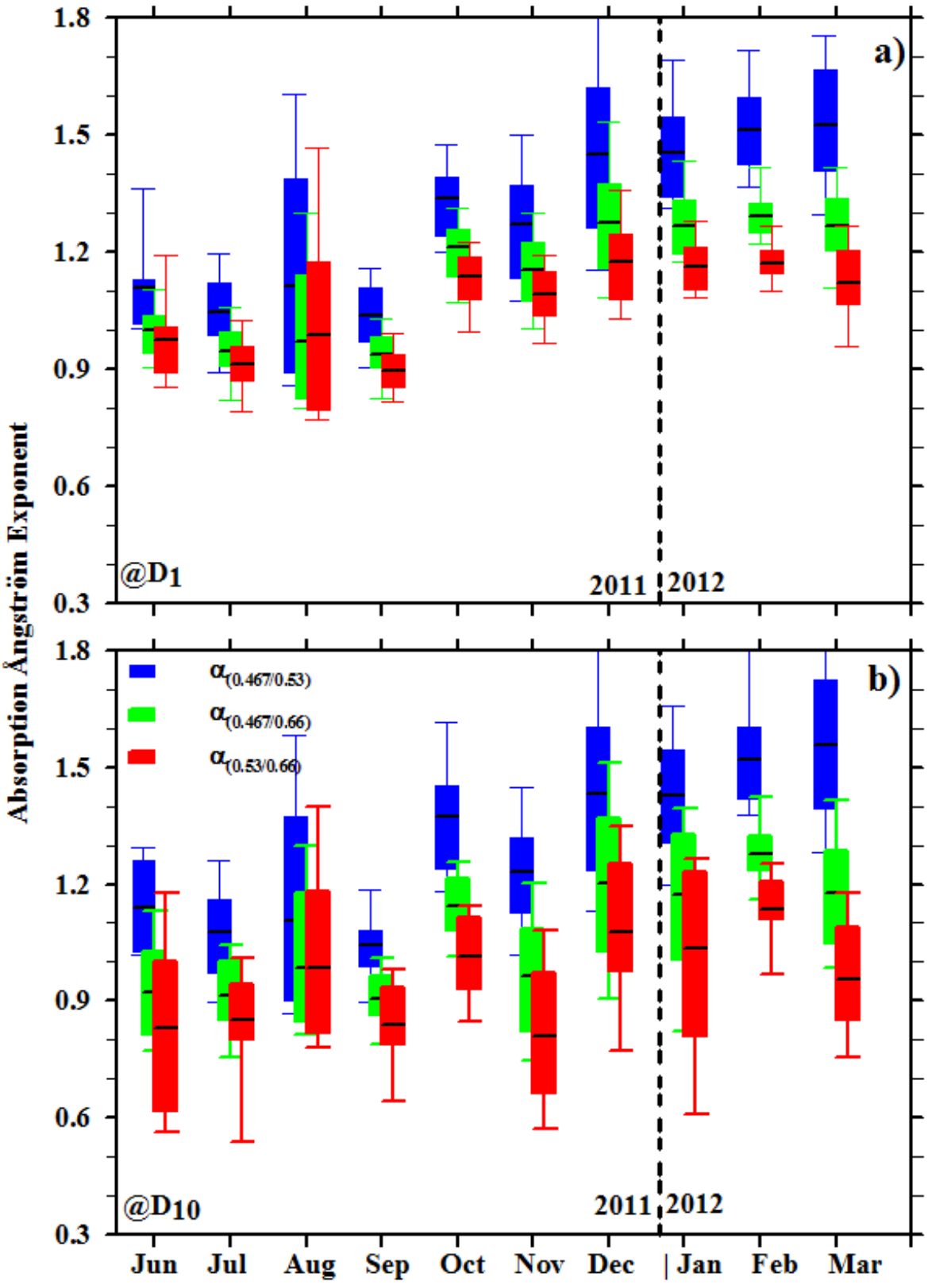

Figure 4: Same as in Figure 3, but for the absorption Ångström exponent.

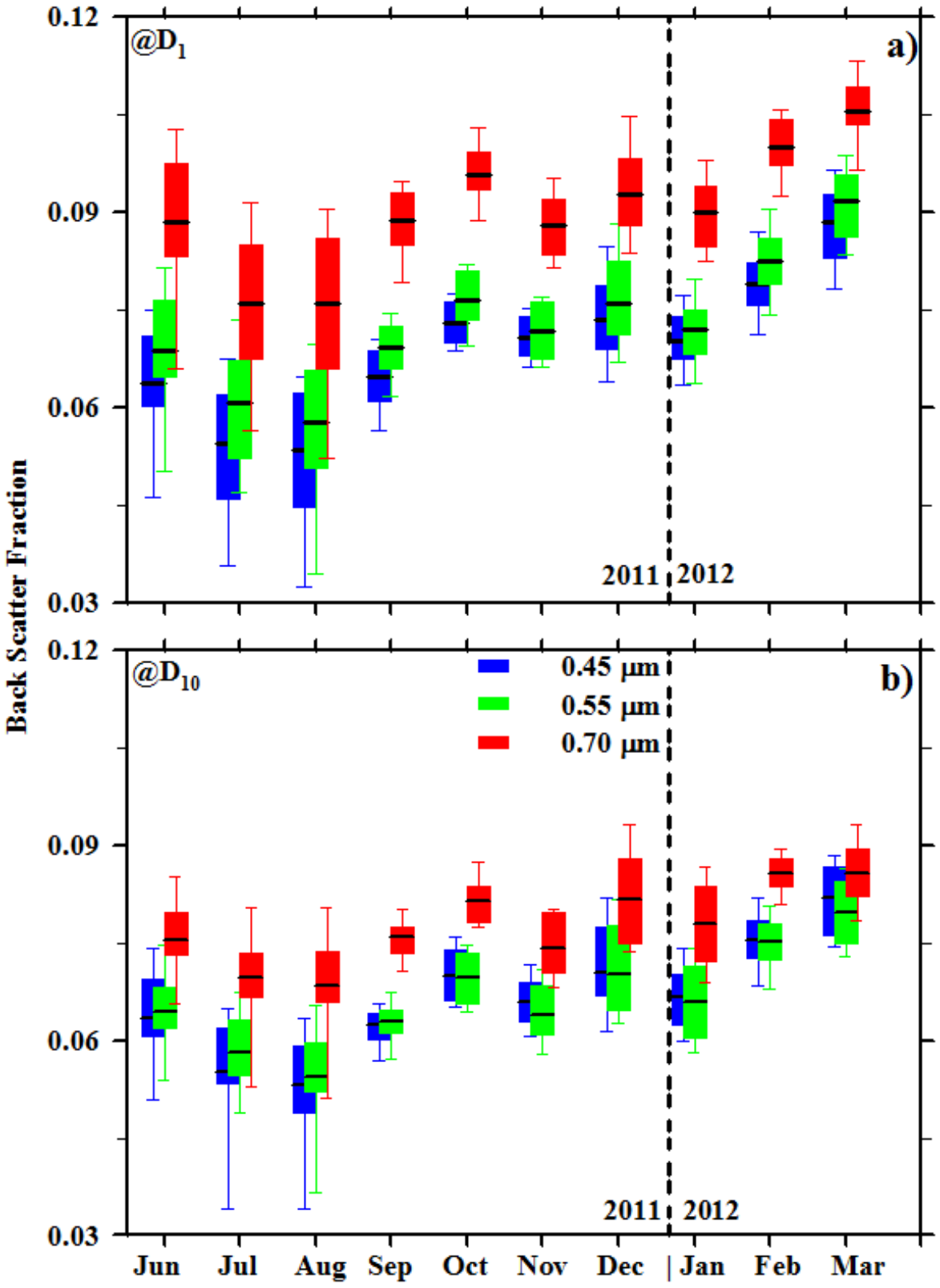

921

922 **Figure 5:** Same as in Figure 3, but for the back-scatter coefficient.

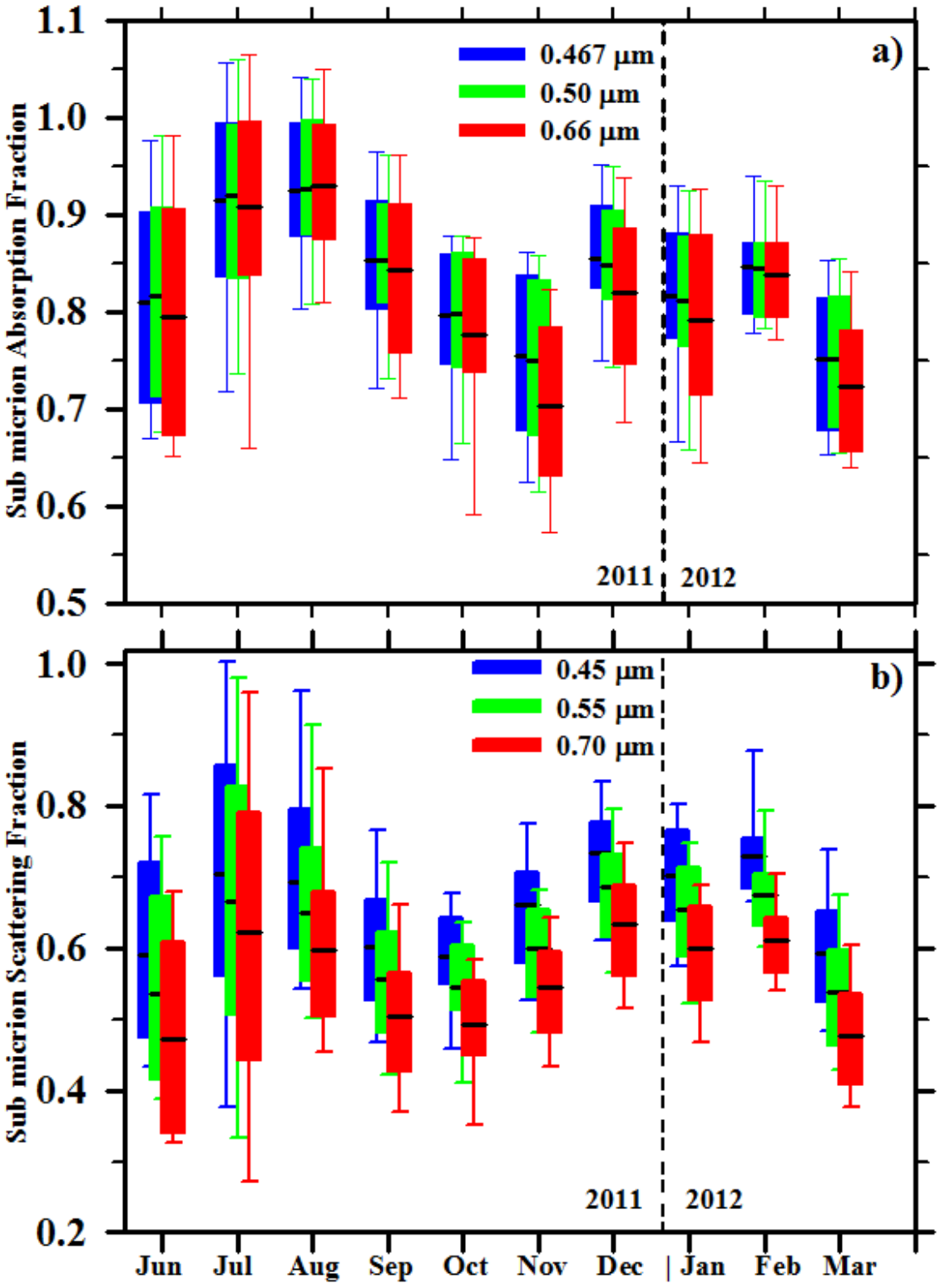

Figure 6: Same as in Figure 3, but for the sub-micron absorption (a) and scattering (b) fraction.

925

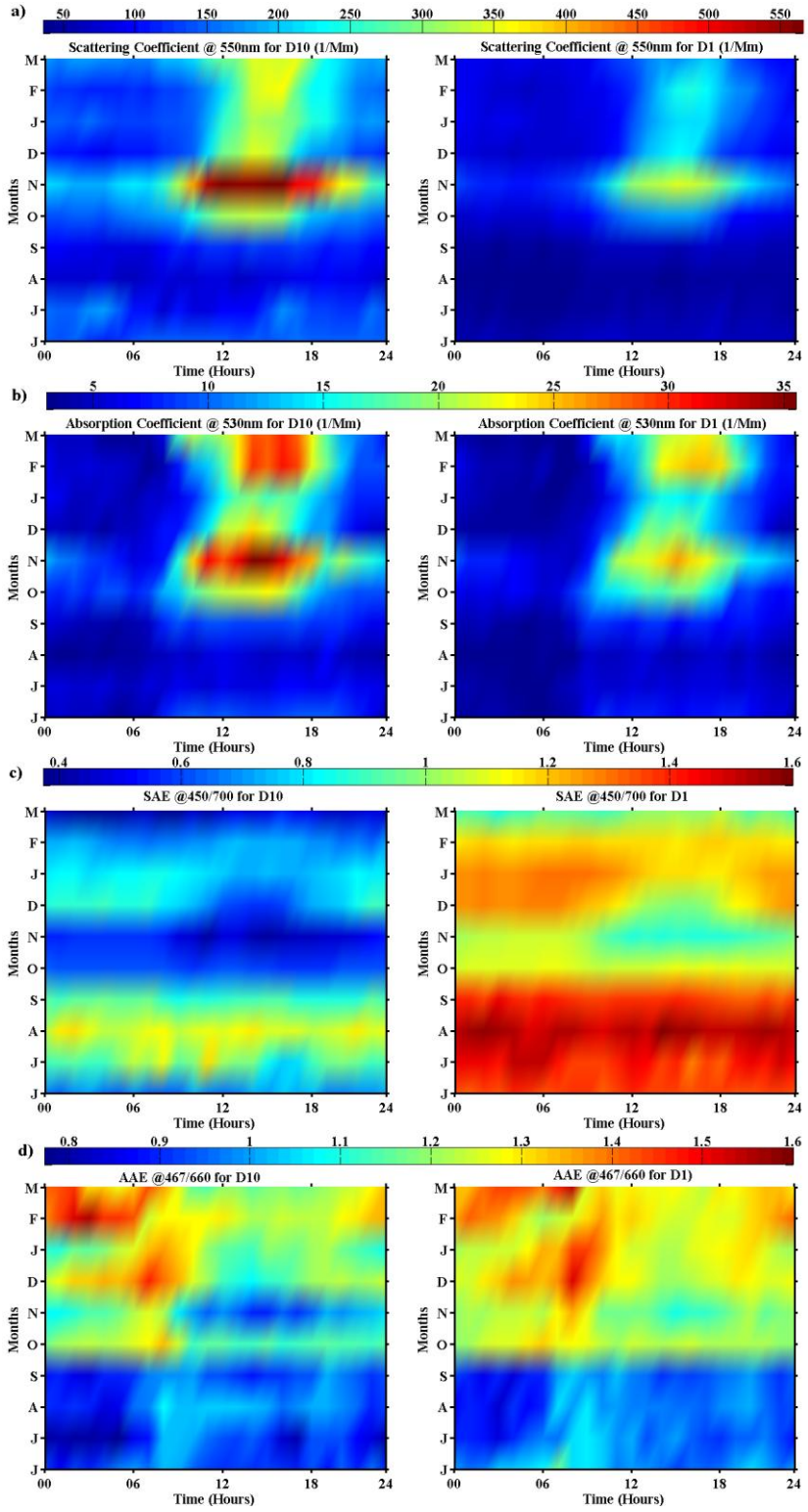

926

927

928

929 **Figure 7:** Monthly mean diurnal variation of (a) scattering coefficient, (b) absorption coefficient,
930 (c) Scattering Ångström Exponent (SAE) and, (d) Absorption Ångström Exponent (AAE) for
931 $D_{10\mu m}$ and $D_{1\mu m}$ size particles.

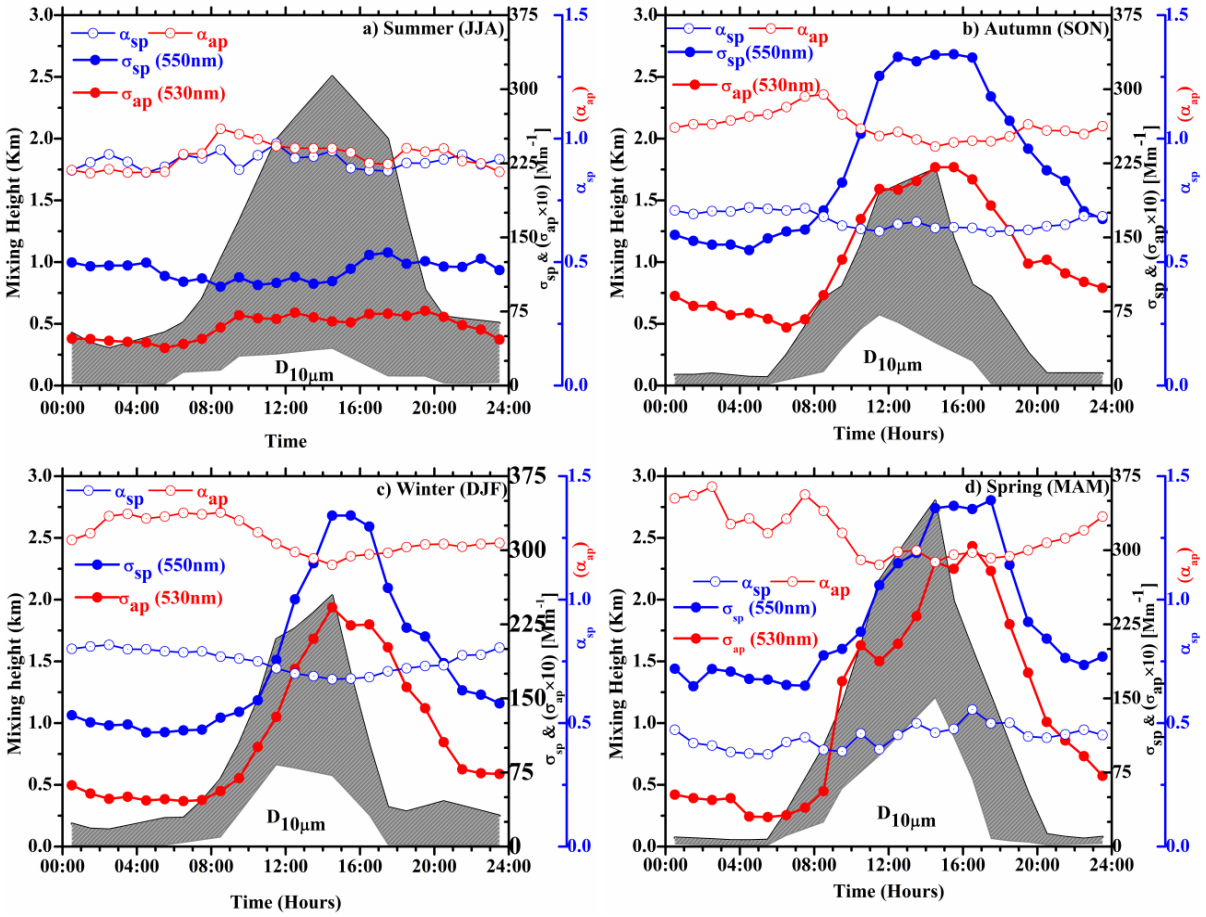

Figure 8: Diurnal variation of the seasonal mean scattering, absorption coefficients, SAE and AAE for $D_{10\mu m}$ particles along with respective variations in the maximum and minimum mixing-layer height over Nainital. The absorption coefficient was multiplied by 10.

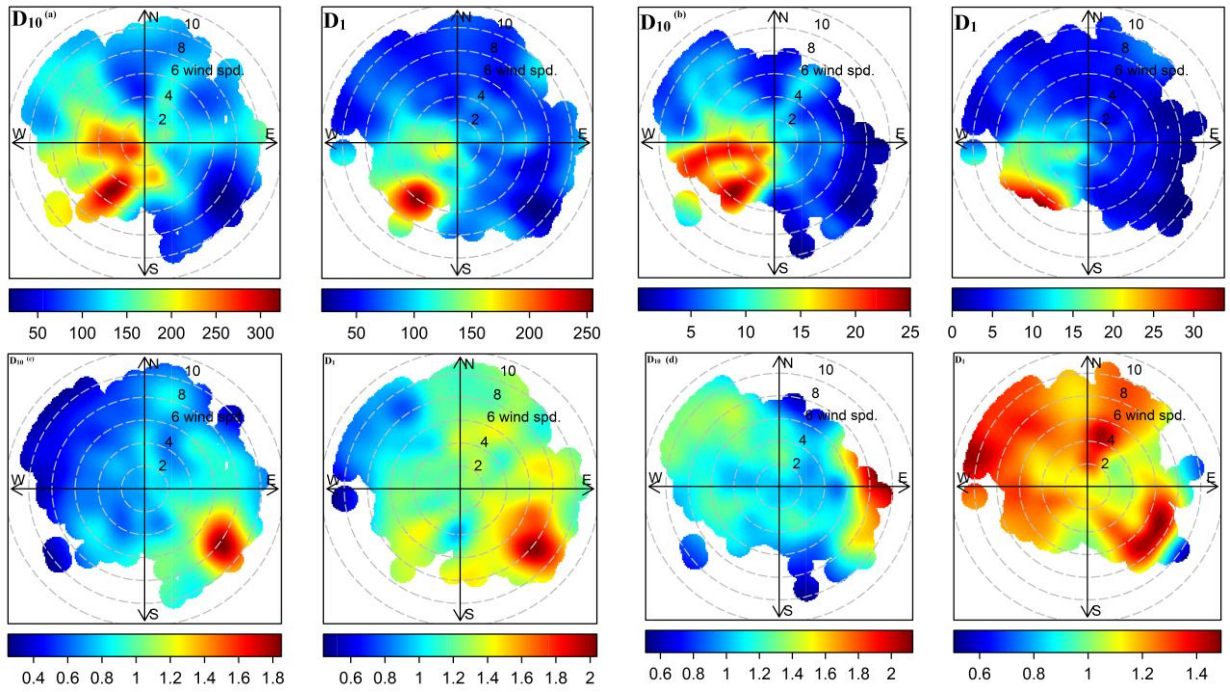

Figure 9: Bivariate plots of the scattering coefficient (a), absorption coefficient (b), scattering Ångström exponent (c) and absorption Ångström exponent (d) for $D_{10\mu m}$ and $D_{1\mu m}$ size groups.

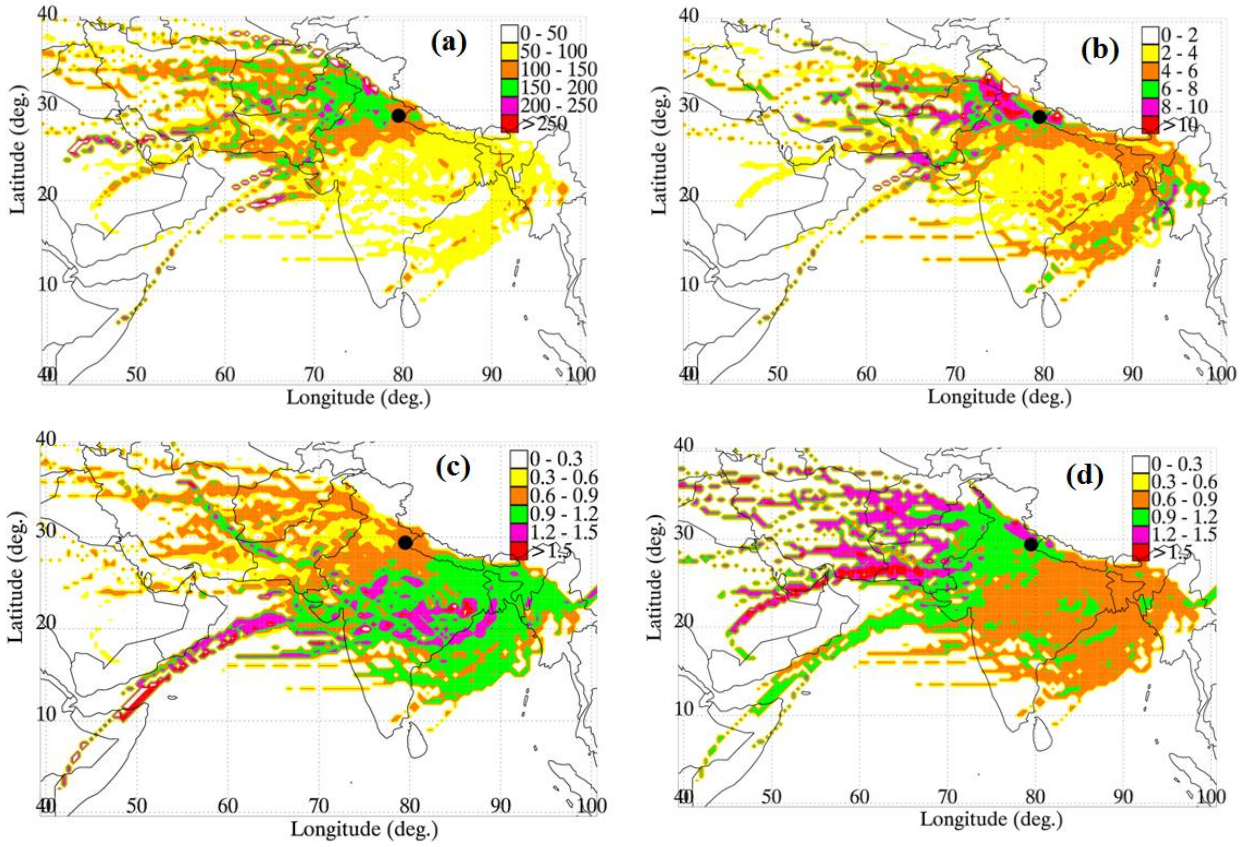

958 **Figure 10**: Concentrated Weighted Trajectory (CWT) maps using 5-days backward trajectories
959 ending at Nainital at 500 m for scattering (a), absorption (b) coefficients, SAE (c) and AAE (d)
960 for $D_{10\mu m}$ particles.

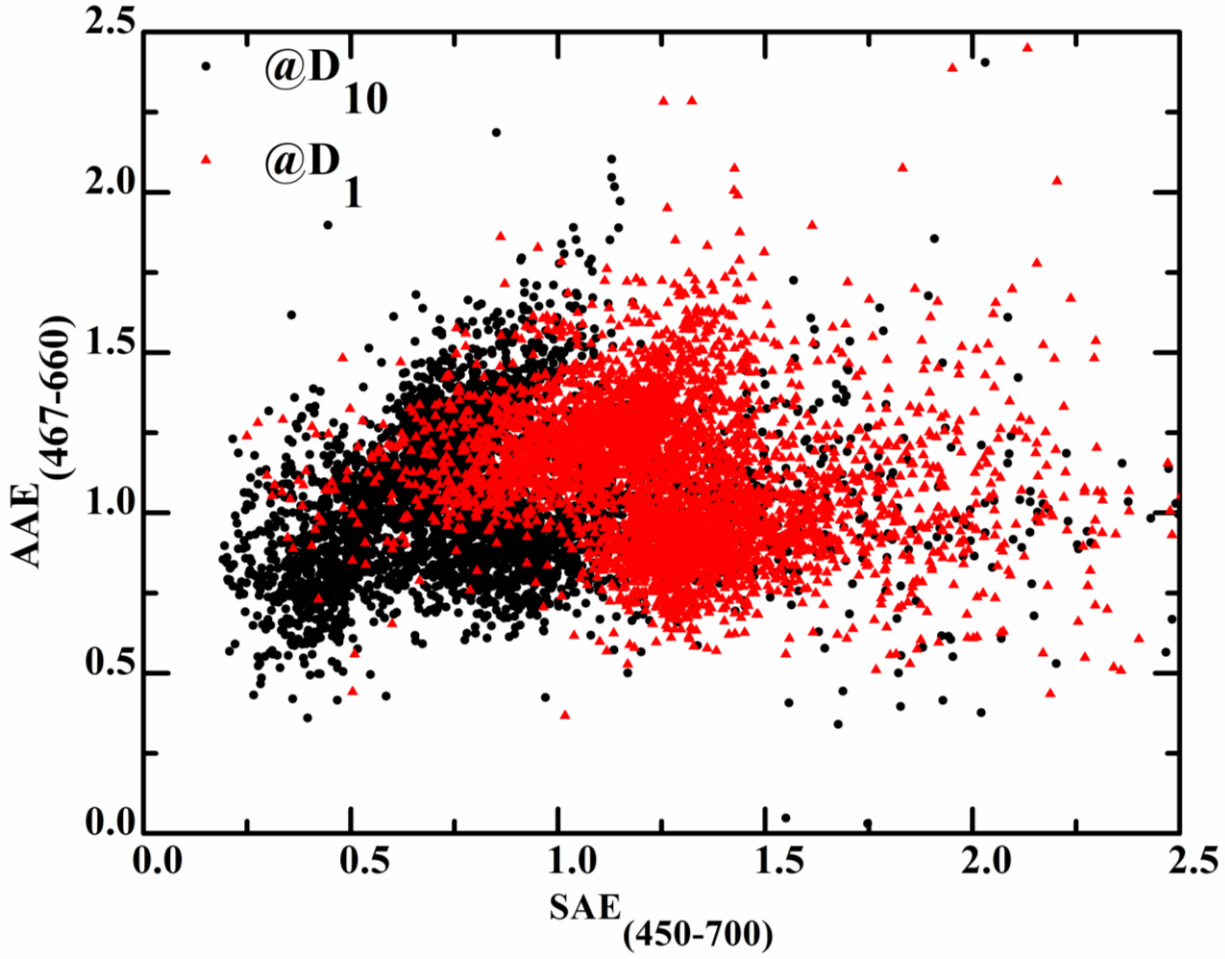

961

962 **Figure 11:** Correlation between scattering and absorption Ångström exponents (hourly-averaged
963 values) at Nainital for $D_{1\mu m}$ and $D_{10\mu m}$ particle-size groups.